# CELL AND MATRIX DYNAMICS DURING BRANCHING MORPHOGENESIS

Jill Shizuko Harunaga

A dissertation submitted to the faculty of the University of North Carolina at Chapel Hill in partial fulfillment of the requirements for the degree of Doctor of Philosophy in the Department of Biology.

Chapel Hill
2014

Approved by:

Kenneth M. Yamada

Robert S. Adelstein

Kerry Bloom

Bob Goldstein

Mark Peifer

## ABSTRACT

JILL S. HARUNAGA. Cell and Matrix Dynamics during Branching Morphogenesis
(Under the direction of Kenneth M. Yamada)

During embryonic development when tissues are particularly plastic, cells within a tissue can often interact with their surrounding extracellular matrix in a reciprocal manner: the cells remodel the matrix, but the matrix can induce signaling and changes in cell behavior, which in turn can affect matrix remodeling to sculpt tissue architecture. A specialized type of extracellular matrix is the basement membrane, which underlies or encapsulates epithelial tissues. We have used the embryonic mouse salivary gland as a model to study cell-basement membrane interactions during branching morphogenesis.

We first focused on whether the cells in contact with the basement membrane (termed outer bud cells) behave differently from cells that remain in contact only with other epithelial cells (inner bud cells). Using a transgenic mouse expressing a photoconvertible fluorescent probe to optically highlight small populations of cells within developing salivary glands, we tracked their migration. The outer cells migrated much more rapidly than the inner cells and each cell population required different proteins for their migration. Therefore, there are two distinct populations of epithelial cells that utilize two different modes of migration in the salivary gland.

We also found that the basement membrane was remarkably dynamic, being remodeled on a local and global scale. There are hundreds of tiny perforations in the basement membrane surrounding the tips of rapidly expanding end buds in embryonic

lung, kidney, and salivary gland. The entire basement membrane also translocates rearward and accumulates to stabilize the duct. Both the micro-perforations and translocation are dependent on myosin II and protease activity. We speculate that the micro-perforations locally increase the distensibility of the basement membrane, allowing directed expansion of the epithelium and basement membrane translocation. Interestingly, the perforations could also allow increased epithelial cell exposure to the mesenchyme, which could stimulate the motility of the outer cells. In summary, we have described a dynamic, bidirectional system in which the cells modify the basement membrane, which in turn affects cell behavior and matrix remodeling to sculpt tissue architecture during branching of the embryonic mouse salivary gland.

## ACKNOWLEDGEMENTS

I would like to thank my family and my husband for their unconditional support and encouragement throughout my pursuit of science. I strive to make you proud. To my advisor and the members of my committee, thank you for challenging me to be a better scientist, I have learned so much from you. To the members of the Yamada laboratory, past and present, I am so grateful for your enthusiasm and scientific thoughtfulness. You all make coming to work an enjoyable and inspiring experience. To my wonderful science teachers and mentors at Kamehameha High School, the Cancer Research Center of Hawaii, and the University of Southern California that started me on this path, I couldn't have done it without you. And thank you to everyone at the National Institutes of Health and the University of North Carolina, Chapel Hill that helps the Graduate Partnerships Program run smoothly.

## TABLE OF CONTENTS

## LIST OF FIGURES

CHAPTER 1:



CHAPTER 2:



CHAPTER 3:

CHAPTER 4:



CHAPTER 5:

## LIST OF ABBREVIATIONS

| | |
|---|---|
| ADAM | A disintegrin and metalloprotease |
| BB-94 | Batimastat |
| Btbd7 | BTB (POZ) domain containing 7 |
| BSA | Bovine serum albumin |
| DMSO | Dimethyl sulfoxide |
| E# | Embryonic day #, eg. E12 means embryonic day 12, 12 days after observation of a vaginal plug |
| EGF | Epidermal growth factor |
| EMT | Epithelial-to-mesenchyme transition |
| FAK | Focal adhesion kinase |
| FGF or FGFR | Fibroblast growth factor or Fibroblast growth factor receptor |
| FRAP | Florescence recovery after photobleaching |
| GAG | Glycosaminoglycan |
| GFP | Green fluorescent protein |
| HB-EGF | Heparin binding epidermal growth factor |
| KikGR | Kikume green-red, a photoconvertible fluorescent probe |
| MMP or MT-MMP | Matrix metalloprotease or Membrane-tethered matrix metalloprotease |
| ROCK | Rho associated protein kinase |
| TIMP | Tissue inhibitor of matrix metalloproteases |

# CHAPTER 1

## Dynamic cell-matrix interactions sculpt morphogenesis

### The basement membrane: a specialized extracellular matrix

The extracellular matrix is a fibrillar mesh of glycoproteins and proteoglycans that surrounds cells in vivo (Hynes and Naba, 2012). Cells have a reciprocal relationship with the extracellular matrix: they synthesize, secrete, and modulate it, while extracellular matrix can signal changes in cell behavior through cell receptors such as integrins (Rozario and DeSimone, 2010). In this manner, cells are highly adaptable to perturbation of their environment, which is particularly important in development. The basement membrane is a specialized extracellular matrix that surrounds epithelial and endothelial tissues, as well as muscle, fat, and Schwann cells (Yurchenco, 2011). It is a thin sheet of highly cross-linked matrix proteins, with a pore size less than 50 nanometers, making it an effective barrier to cell migration that compartmentalizes tissues (Rowe and Weiss, 2008; Yurchenco, 2011). The properties of each basement membrane are dependent on its molecular composition of matrix proteins, which show differential developmental and tissue-specific expression patterns (Candiello et al., 2010; Halfter et al., 2013; Hynes and Naba, 2012; Yurchenco, 2011). These facts make the study of cellular interactions with the basement membrane difficult, since embedding cells in basement membrane extract or laminin gels does not recapitulate the covalent structure, rigidity, composition, and dynamic changes of a native basement membrane.

The basement membrane is composed of laminin, nidogen, heparan sulfate proteoglycans, and collagen IV (Yurchenco, 2011). These are very large insoluble proteins that have been evolutionarily conserved from metazoans through mammals (Hynes and Naba, 2012). The self-assembly of the basement membrane is initiated by laminin assembly on the cell surface through adhesion to integrin and dystroglycan receptors (Li et al., 2005; McKee et al., 2007; Yurchenco, 2011). Laminin assembly appears to seed accumulation of the other basement membrane components, which begin to accumulate with the assembly of laminin (Kelley et al., 2014; Yurchenco, 2011). Because the initiation of the laminin network is dependent on cell adhesion, basement membrane organization can be modulated by the intracellular cytoskeletal network through cell-matrix adhesions (Colognato et al., 1999). The collagen IV network assembles via intramolecular covalent bonds, which provides structural integrity and mechanical strength to the basement membrane (Khoshnoodi et al., 2008; Poschl et al., 2004). Nidogen and heparan sulfate proteoglycans link the laminin and collagen IV networks together, forming a dense, 50-100 nanometer thick meshwork of extracellular matrix, providing a sink for growth factors as well as structural integrity to the tissue it surrounds (Rowe and Weiss, 2008; Yurchenco, 2011). Basement membranes play multiple important roles in morphogenesis, with functions that include providing tissue structural support and boundaries, mediating growth factor signaling, and providing polarity cues (Rozario and DeSimone, 2010; Yurchenco, 2011).

**The embryonic salivary gland as a model for tissue-matrix interactions**

Branching morphogenesis is an essential developmental process by which several mammalian organs such as the lung, kidney, mammary and salivary glands gain epithelial surface area for secretion or adsorption (Harunaga et al., 2011; Kim and Nelson, 2012; Patel et al., 2006). The process begins with a single epithelial bud surrounded by basement membrane and dense mesenchyme. The epithelium expands and divides through repetitive rounds of branching to form a highly arborized structure, which allows for maximal surface area confined within a small space. As the epithelial tissue expands and branches, it remains encapsulated by a basement membrane (Rozario and DeSimone, 2010; Timpl and Dziadek, 1986). Because the basement membrane provides such important cues, and because the epithelium expands rapidly during development, the basement membrane must also be rapidly remodeled to accommodate the expanding tissue in order to continue to surround the epithelium.

Using the embryonic *Mus musculus* (mouse) submandibular salivary gland (or simply, salivary gland) as a model, we are interested in the coordination of tissue morphogenesis and the basement membrane during branching. We suspected that this process might be highly dynamic and would require a model system in which we could do whole-organ live imaging. The salivary gland has been used as a model for branching morphogenesis since 1953 and has provided insight into the development of several other organs (Andrew and Ewald, 2010; Grobstein, 1953; Kim and Nelson, 2012). This organ can be excised from the embryonic mouse at embryonic day 12 or E12 (12 days following conception) and cultured ex vivo for at least 72 hours on top of a filter floating on media (Fig. 1.1) (Patel et al., 2006). Branching is closely recapitulated ex vivo,

beginning at E12.5 when the single epithelial bud becomes divided by clefts; the clefts then elongate to delineate ducts; this branching is followed by lumen formation and differentiation beginning at E15 (Patel et al., 2006). Salivary glands cultured ex vivo are ideal for fluorescence live imaging because they flatten more than the other branched organs while still maintaining their three-dimensional shape, allowing for crisper images with less background fluorescence. Our ex vivo approach allows us to study how cell-mediated remodeling of a native basement membrane affects tissue architecture and reciprocally, how basement membrane affects cell dynamics in a whole organ.

***Branching morphogenesis requires basement membrane proteins***

Several extracellular matrix proteins including collagen I, III, IV, heparan sulfate proteoglycans, fibronectin, laminin 1 and alpha 5, as well as cell-matrix adhesion proteins including integrin β1, α3, α5, and α6 are necessary for several developmental processes including branching morphogenesis (Cutler, 1990; Fukuda et al., 1988; Harunaga et al., 2011; Kadoya et al., 1995; Kashimata and Gresik, 1997; Menko et al., 2001; Patel et al., 2007; Rebustini et al., 2007; Sakai et al., 2003; Wei et al., 2007). These and other studies indicate that in addition to requiring basement membrane proteins, the cells also need to be able to adhere to the basement membrane for survival and proper morphogenesis. In experiments completed almost 50 years ago, collagenase treatment of branched epithelial rudiments that had been removed from the mesenchyme resulted in regression of clefts in the embryonic salivary gland, reducing the epithelium to a round flat disk (Banerjee et al., 1977; Grobstein and Cohen, 1965). The absence of clefts appeared to have no effect on the health of the epithelium, since it continued to increase in area (Grobstein and Cohen, 1965). This result in combination with the known localization of collagen

suggests that collagen, which is absent from the “morphologically active” end buds, is a stabilizing component in the cleft and duct regions (Grobstein and Cohen, 1965; Kallman and Grobstein, 1965). In fact a collagenase inhibitor can stimulate cleft formation and increases collagen-like fibrils on the surface of the salivary gland epithelium early in development (Nakanishi et al., 1986). Conversely, inhibition of collagen synthesis, but not inhibition of collagen crosslinking, inhibited branching in both the salivary gland and lung (Spooner and Faubion, 1980).

The importance of glycosaminoglycans (GAGs) such as chondroitin sulfates or heparan sulfate, and their extracellular matrix proteoglycans including perlecan, in branching has also been demonstrated in the embryonic salivary gland. Complete removal of the GAGs results in a severe inhibition of salivary gland branching morphogenesis (Thompson and Spooner, 1982). The other main components of the basement membrane, laminin and fibronectin, are also required for branching morphogenesis (Rebustini et al., 2007; Sakai et al., 2003). Laminin is necessary for development: treatment of embryonic lungs or salivary glands with laminin function-blocking antibody decreased branching (Kadoya et al., 1995; Schuger et al., 1990). Mice deficient for an isoform of laminin, Lama5, exhibit a significant delay in branching of the salivary gland, and once branching does commence, the epithelium appears disorganized and lumen formation is disrupted (Rebustini et al., 2007). Fibronectin is required for branching of the embryonic salivary gland (Sakai et al., 2003), but excess fibronectin and its associated receptor α5β1 integrin inhibit branching (Joo and Yamada, 2014).

Just as basement membrane proteins are required for survival and morphogenesis of branched organs, extracellular matrix-modifying proteins such as proteases and their

regulators are important as well. Proteases from the metalloprotease family are the major players in extracellular matrix remodeling, including matrix metalloproteases (MMPs) and a disintegrin and metalloprotease with thrombospondin motifs (ADAMs) (Lu et al., 2011). This very large family of proteases cleaves a wide range of matrix proteins; they also act on protease precursors and growth factors, activating them through cleavage. Their activity is often redundant, making it difficult to pinpoint specific functions (Lu et al., 2011). The *Mmp-14* knock-out mouse displays decreased branching of the salivary gland and significantly reduced collagen metabolism (Holmbeck et al., 1999; Oblander et al., 2005). *Adam17*-null embryos exhibit decreased terminal bud numbers and increased extracellular matrix accumulation in their salivary glands compared to wild-type controls (Melnick and Jaskoll, 2000). Finally, MMP-2 and MMP-3 activities have been shown to mediate side and primary branching, respectively, in murine mammary gland organoid cultures (Wiseman et al., 2003).

As important as protease activity is to morphogenesis, their activity must carefully be balanced since excess proteolytic activity can be detrimental. Overexpression of MMP-3 leads to increased mammary gland side branching, potentially through a partial epithelial-to-mesenchyme transition (EMT) to allow invasion of the epithelium into the fat pad, and eventually tumor formation (Lochter et al., 1997a; Lochter et al., 1997b; Sternlicht et al., 1999). The loss of tissue inhibitor of matrix metalloproteases 3 (TIMP3), which results in excessive protease activity, inhibits branching morphogenesis in the embryonic mouse lung (Gill et al., 2006).

### *Actomyosin contractility in branching morphogenesis*

The importance of actomyosin contractility in cell migration and tissue morphogenesis is well documented (Vicente-Manzanares et al., 2009). It can generate tensile forces within the cell that can be transmitted through cell-matrix or cell-cell adhesions to effect global changes in tissue shape and extracellular matrix organization (Fischer et al., 2009; Mammoto and Ingber, 2010; Schwartz, 2010; Simoes Sde et al., 2014). Non-muscle myosin II (referred to below as myosin II) is a contractile actin-binding protein that can also self-associate to form bipolar filaments along actin filaments. Myosin II induces contraction of the actin filaments though ATP-dependent conformational changes in its head and neck region, sliding the filaments together (Landsverk and Epstein, 2005). Activation and regulation of ATP hydrolysis is dependent on phosphorylation of the regulatory light chains that associate with the neck region of the myosin II heavy chain (Adelstein and Conti, 1975). Studies of the lung (Moore et al., 2005; Plosa et al., 2012), salivary gland (Daley et al., 2012; Daley et al., 2009), and mammary gland (Ewald et al., 2008; Ewald et al., 2012) have demonstrated a requirement for actomyosin contractility in branching morphogenesis, as shown in studies utilizing several well-known pharmacological inhibitors of myosin II contractility (Kim and Nelson, 2012), including the Rho (ROCK) inhibitor Y27632 (Uehata et al., 1997) and the myosin light chain kinase inhibitor ML-7 (Saitoh et al., 1987), both of which inhibit kinases that activate the myosin II regulatory light chain, or the myosin II ATPase inhibitor blebbistatin (Limouze et al., 2004). These pharmacological inhibitors directly or indirectly act on all three isoforms of myosin II.

Branching is inhibited in embryonic mouse lungs with ROCK inhibitor treatment without affecting proliferation rates, resulting in a decreased number of enlarged end buds that fail to form clefts (Moore et al., 2005). Conversely, treatment with cytotoxic necrotizing factor-1 to increase Rho activity and contractility has a biphasic effect on lung branching, increasing the number of end buds at low doses and decreasing the bud number at high concentrations (Moore et al., 2005). Pharmacologically modulating the contractility of the lung also increases the thickness of the basement membrane, which is typically thinner at the tips of the end buds (Moore et al., 2005). How tissue contractility changes the thickness of the basement membrane is unknown, but it is postulated that protease activity is tension-mediated (Moore et al., 2005). Increased cellular tension could decrease protease activity, as it has been shown that increased tension from cell spreading and integrin binding eventually decreases MMP2 activity by decreasing expression of MT1-MMP in endothelial cells (Moore et al., 2005; Yan et al., 2000). Myosin II also regulates cell shape and branch formation in the lung (Plosa et al., 2012). Treatment with blebbistatin results in a decrease in the organization of the epithelial cells in the stalk region, which is analogous to the duct region in the salivary gland, and an increase in cell size (Plosa et al., 2012). Whether the change in cell size and organization is related to the changes in basement membrane thickness observed previously is unknown.

In the developing mouse salivary gland, blebbistatin or Y27632 treatment inhibits branching morphogenesis by prohibiting cleft progression, though clefts are still able to initiate (Daley et al., 2012; Daley et al., 2009). ROCK-mediated actomyosin contractility is required to assemble fibronectin in the clefts to drive progression of the cleft (Daley et

al., 2009). Localized fibronectin assembly also induces cell proliferation to expand the bud outward as the cleft progresses inward (Daley et al., 2009). In addition to mediating assembly of fibronectin in the basement membrane, ROCK regulates basement membrane deposition and polarization of the peripheral epithelial cells in a myosin II-independent manner (Daley et al., 2012). Treatment with Y27632 but not blebbistatin induces ectopic deposition of basement membrane components within the epithelial bud instead of just at the epithelial-mesenchyme interface; this disrupts polarization of the outer bud epithelial cells, which usually are columnar-shaped and well-organized along the basement membrane (Daley et al., 2012; Onodera et al., 2010).

In mammary gland organoid cultures embedded in basement membrane extract, ML-7 treatment prevented ductal initiation, and cells were able to form cysts and make lumens but remained unbranched (Ewald et al., 2008). Interestingly, ROCK inhibition did not negatively affect branching of the organoids and in some cases increased branching, but the resulting organoids were disorganized with several small lumens, instead of one continuous lumen (Ewald et al., 2008). Loss of ROCK resulted in decreased ZO-1 and E-cadherin staining, suggesting a decrease in cell polarity and cell-cell adhesion caused the disorganized organoid phenotype (Ewald et al., 2012). This finding is consistent with the myosin II-independent function of ROCK in polarized deposition of basement membrane in the salivary gland (Daley et al., 2012). The difference in the amount of branching observed with ROCK inhibition in mammary and salivary glands demonstrates a mechanistic difference in how the buds are divided; in the salivary gland epithelium, clefts progress into the epithelium as the buds expand outward; conversely, in the

mammary glands the end buds appear to collectively invade outward (Daley et al., 2009; Ewald et al., 2008; Ewald et al., 2012; Onodera et al., 2010).

***Cell motility during branching morphogenesis***

Branching is a complex, dynamic process that requires extensive remodeling of tissue, and the epithelial cells display surprisingly high levels of cell motility. These cell movements during branching morphogenesis have been suggested to contribute to the plasticity of tissues during the rapid architectural rearrangements of early organ formation. Confocal timelapse microscopy of GFP-adenovirus infected salivary glands revealed extensive random, individual cell motility of the epithelial cells during development (Larsen et al., 2006). The epithelial cells of the developing mouse mammary gland and *Drosophila melanogaster* (*Drosophila*) trachea also display a high degree of cell motility (Ewald et al., 2008; Ewald et al., 2012; Metzger and Krasnow, 1999). The epithelial cells of the developing kidney also move, though significantly less than observed in the salivary gland (Shakya et al., 2005). Higher-power imaging showed that salivary gland epithelial cells migrate as single cells in random patterns (Larsen et al., 2006), but epithelial cells from the mammary gland migrate both individually and as collective groups (Ewald et al., 2008; Ewald et al., 2012). Preliminary observations suggested that the salivary gland outer bud and cleft epithelial cells that are in contact with the basement membrane are especially motile.

The epithelial cell motility that occurs transiently during salivary gland branching morphogenesis is developmentally regulated, and it ceases when glands mature to form the stable epithelial cell–cell adhesions characteristic of adult organisms (Hieda et al., 1996; Larsen et al., 2006). The cell–cell adhesion complexes that comprise the classical

adherens, tight, and desmosome-based junctions of very early epithelia are lost when oral epithelial cells undergo branching morphogenesis to form buds (Hieda et al., 1996; Kadoya and Yamashina, 1993). In post-natal branching mammary glands, adherens and tight junctions also appear to be lost during branching morphogenesis, although desmosomes remain (Ewald et al., 2012). Because the cells are so motile, the tissue is likely extremely plastic throughout development, and perhaps the basement membrane surrounding the remodeling tissue is also highly dynamic.

**Basement membrane remodeling in development**

Extracellular matrix remodeling rates are especially high during development, wound repair, and cancer metastasis (Daley et al., 2008). During development, as tissues undergo dynamic changes in size and shape, the basement membrane must also be dynamic to accommodate and mold the developing tissue. Here we focus on previous research on basement membrane remodeling in the development of several model systems, with particular emphasis on branched organs. Remodeling of the basement membrane through protein synthesis and deposition, proteolytic removal, physical movement, or crosslinking can alter cell motility, shape, polarity, and adhesion (Gjorevski and Nelson, 2009; Rozario and DeSimone, 2010; Yurchenco, 2011). In this intriguing bidirectional signaling system, a small number of cells can modulate the behavior of cells locally, and more globally, sculpt an entire tissue by simply modifying the chemical, mechanical, or topographical cues of the basement membrane. This feedback regulatory mechanism between cells and the basement membrane also allows cells and tissue to adapt quickly to changes in their environment (Lu et al., 2011).

***Sculpting and stabilizing tissue***

Historically, the basement membrane was typically thought to be predominantly structural, providing support to the epithelial tissue it surrounds (Rozario and DeSimone, 2010). While more recently the basement membrane has been shown to be a dynamic structure with several other functions in addition to structural support, how tissues organize and remodel their basement membranes to dictate form and function remains unclear. Several cell types can orient and slide extracellular matrix fibers, which may help to guide and stabilize tissue architecture.

One of the best documented instances of basement membrane shaping of tissue architecture is in the *Drosophila* egg chamber (Bilder and Haigo, 2012; Horne-Badovinac, 2014). The whole egg chamber rotates to orient the basement membrane as the oocyte matures and elongates along the anterior/posterior axis to change from a round spherical shape to an oval shape (Haigo and Bilder, 2011). During this maturation period, the entire egg chamber rotates along its circumferential axis, orienting the surrounding, stationary basement membrane into polarized fibrils (Haigo and Bilder, 2011). This polarized basement membrane then acts as a "molecular corset" that physically constricts the expansion of the egg chamber to the anterior/posterior axis, guiding elongation of the egg (Bilder and Haigo, 2012). In mutant flies lacking the *Drosophila* integrin βPS or the basement membrane components collagen IV or laminin, the egg chamber does not elongate and the basement membrane does not become polarized, indicating that the interaction between the epithelial cells and the basement membrane is required (Haigo and Bilder, 2011). Treatment of the elongated egg chamber with collagenase to disrupt the basement membrane, but not Latrunculin A which depolymerizes actin filaments,

results in rapid rounding of the egg, suggesting it is the basement membrane and not the cells themselves that maintains the elongated structure of the tissue (Haigo and Bilder, 2011). Tissue rotation induces basement membrane polarization, and the basal actin filaments in the epithelial cells become planar polarized along the same axis as the basement membrane (Gutzeit et al., 1991). Cell migration of the underlying follicle cells is also required for the polarization of the basement membrane (Lewellyn et al., 2013). However, the typical Wnt-mediated planar cell polarity signaling pathways are not required; instead the egg chamber rotation seems sufficient to orient both the basement membrane and the basal actin filaments (Bilder and Haigo, 2012; Viktorinova et al., 2009). Directed deposition of collagen IV by the rotating planar polarized epithelial cells also contributes to the polarization of basement membrane structure (Lerner et al., 2013), which indicates there are multiple facets of regulation (Horne-Badovinac, 2014).

Murine mammary gland acini assembled from single cells also rotate when they are imbedded in basement membrane extract (Tanner et al., 2012; Wang et al., 2013). The rotation is accompanied by planar polarized actin on the basal surface of the epithelial cells and an oriented laminin matrix similar to that observed in the *Drosophila* egg chamber (Tanner et al., 2012; Wang et al., 2013). This indicates that entire tissue rotation could be used by several organisms to orient basement membrane. In the mammary gland this process requires actomyosin contractility and the polarity protein, PAR3 (Wang et al., 2013). The rotation halts upon maturation of the acini, but restarts when the basement membrane is exogenously disrupted (Wang et al., 2013). Interestingly, malignant cells did not rotate or organize the basement membrane, resulting in abnormally shaped acini (Tanner et al., 2012; Wang et al., 2013).

In addition to the recent demonstrations that whole tissue movements can physically orient basement membrane, it had been previously observed that the basement membrane varies in thickness in different locations surrounding the epithelium of the branching lung, mammary and salivary glands (Bernfield and Banerjee, 1982; Fata et al., 2004; Mammoto and Ingber, 2010; Mollard and Dziadek, 1998; Moore et al., 2005; Silberstein and Daniel, 1982). In the mammary gland, the basement membrane at the tips of the expanding terminal end buds can be 10 times thinner than the basement membrane along the forming ducts (Fata et al., 2004). Salivary glands treated with collagenase exhibit regression of the clefts and decreased branching (Banerjee et al., 1977; Grobstein and Cohen, 1965). Such clefts divide an epithelial bud into two buds, eventually progressing to a duct during branching morphogenesis of the salivary gland. This regression suggests that the thicker basement membrane found in clefts and ducts could be supporting and stabilizing these structures. Ingber suggests that the varying thickness and thus stiffness of basement membrane exposes the epithelium to varying local force anisotropies, permitting directed tissue expansion only in areas where the basement membrane is thinnest (Mammoto and Ingber, 2010; Moore et al., 2005).

How the differences in basement membrane thickness are established in the first place has yet to be completely elucidated, but it has been shown that fibronectin appears to assemble and translocate into the clefts of developing salivary glands (Larsen et al., 2006; Sakai et al., 2003). This localized assembly is driven by Rho kinase (ROCK) mediated actomyosin contractility and focal adhesion kinase (FAK) activation (Daley et al., 2009; Daley et al., 2011). The assembled fibronectin is translocated into the cleft with newer fibronectin assembling behind it, recruiting other structural proteins such as

collagen III and creating a physical wedge to promote cleft progression (Nakanishi et al., 1988). Perhaps localized assembly and translocation of the basement membrane could create the differences in basement membrane thickness and force anisotropies during branching morphogenesis. Additionally, there could be differences other than thickness between the tip and duct regions in branching organs, such as the amount of crosslinking and composition of the basement membrane that contribute to the architecture of the tissue. For example, the thinner basement membrane at the tips of mammary end buds contains more hyaluronic acid than the thicker basement membrane around the ducts, which likely affects local signaling (Hinck and Silberstein, 2005; Silberstein and Daniel, 1982).

Variations in the rate of local deposition and degradation were also proposed to contribute to the differences in thickness of the basement membrane surrounding the salivary gland. In a classic pulse-chase experiment in 1982, Bernfield and Banerjee measured the rates of uptake and disappearance of radiolabeled glycosaminoglycans in the basement membrane during branching morphogenesis of the mouse salivary gland (Bernfield and Banerjee, 1982). They found that while the radiolabelled GAGs incorporated first at the tips of end buds, upon removal of the label, the radiolabelling disappeared quickly at the tips and persisted in the clefts, suggesting that the rates of deposition and turnover are much higher at the distal tip of the end buds than the clefts (Bernfield and Banerjee, 1982). Localized turnover of the basement membrane by proteolysis is another way in which the basement membrane could be thinned specifically at the tips of end buds. In the lung, kidney, and mammary and salivary glands, matrix

metalloproteases or MMPs have been shown to be required branching (Fata et al., 2004; Lelongt et al., 1997; Oblander et al., 2005).

***Inducing proliferation and dynamic cell motility***

In addition to removing a physical impediment to branching, proteolysis can release bioactive extracellular matrix fragments or growth factors bound in the basement membrane that increase proliferation, motility, and overall branching of the organ (Ortega and Werb, 2002; Patel et al., 2007; Rebustini et al., 2009; Sternlicht et al., 2006). In a feed-forward pathway, MT2-MMP (membrane-type 2 matrix metalloprotease or MMP15) degrades collagen IV in the basement membrane surrounding branching salivary glands, releasing bioactive NC1 domains, which signal through β1 integrin and AKT to increase collagen IV synthesis and the expression of MT2-MMP, the fibroblast growth factor receptor (FGFR), and heparin binding epidermal growth factor (HB-EGF), stimulating epithelial proliferation (Rebustini et al., 2009). Addition of NC1 domains or exogenous HB-EGF does not rescue the branching defect in glands that have been treated with a broad protease inhibitor or MT2-MMP siRNA (Rebustini et al., 2009). This suggests that both the physical removal of basement membrane and the released NC1 domains are required to create a permissive environment for successful branching morphogenesis. Modifications of the basement membrane proteins themselves can also affect cell signaling. Cleavage of the heparin sulfate from its proteoglycan releases basement membrane-bound growth factors like fibroblast growth factor 10 (FGF10), and the type of sulfation modification on the heparin sulfate can modulate the activity of FGF10 towards proliferation, bud expansion, duct elongation or differentiation (Patel et al., 2007; Patel et al., 2008).

A basement membrane-associated protein, fibronectin, can signal directly through integrin α5β1 in the clefts of the embryonic mouse salivary gland and alter cell motility and adhesion. Localized assembly and accumulation of fibronectin rapidly induces Btbd7 [BTB (POZ) domain containing 7] at the base of the clefts, which then up-regulates the transcription factor Snail2 while down regulating E-cadherin (Onodera et al., 2010; Sakai et al., 2003). This is one of the first examples of an extracellular matrix protein directly affecting transcription in the nucleus. The down-regulation of E-cadherin results in decreased cell adhesion at the base of the clefts, which cooperates with Snail2 to induce a more motile population of cells, allowing for dynamic cell rearrangements and progression of the cleft through the epithelium (Onodera et al., 2010). As basement membrane proteins can induce cell migration, they can also reduce migration. During *Xenopus laevis* gastrulation, assembly of fibrillar fibronectin is required for blastocoel roof thinning and epiboly but actually slows down convergent extension (Rozario et al., 2009). This suggests that different cell types can respond differently to the same basement membrane protein at different times, adding additional layers of regulation to cell-matrix interactions.

Topography and the absence of basement membrane may also have a role in regulating proliferation and differentiation. Several electron microscopy studies conducted in the 1970s showed discontinuities in the basement membrane at the tips of the end buds in the developing tooth bud, lung, kidney, and salivary gland (Bluemink et al., 1976; Cutler, 1977; Cutler and Chaudhry, 1973; Lehtonen, 1975; Slavkin and Bringas, 1976). The epithelium contacts the mesenchyme in the areas where the basement membrane is absent, potentially inducing cyto-differentiation (Cutler, 1980; Cutler and

Chaudhry, 1973). These contacts are transient and occur at the tips of the epithelial end buds (Cutler and Chaudhry, 1973). The tips of the rapidly expanding end buds are considered areas of high morphogenic potential, exhibiting increased cell proliferation compared to areas adjacent to the clefts in the developing lung (Mollard and Dziadek, 1998). Breaks in the basement membrane also occur in adult organs such as the intestine and lymph vessels (Komuro, 1985; Pflicke and Sixt, 2009; Trier et al., 1990). However, how these breaks in the basement membrane form and how epithelial-mesenchyme interactions may induce differentiation or branching remains unknown.

***Inducing cell invasion***

Cells also need to physically traverse the basement membrane during development to establish new tissue or to make connections between existing ones (Kelley et al., 2014). This process is especially difficult because the basement membrane usually functions as a barrier to migration, compartmentalizing different cell types. And instead of simply modifying the intact basement membrane as we have described in the previous sections, invading cells and tissue must actually breach a very tough, dense sheet of extracellular matrix. While this process occurs normally in many developmental processes, it can become mis-regulated in pathological conditions, such as cancer metastasis (Fata et al., 2004; Lu et al., 2011; Rowe and Weiss, 2008).

A particularly well-documented example of basement membrane crossing is the invasion of the anchor cell in *Caenorhabditis elegans* (*C. elegans*) uterine-vulval attachment (Sherwood and Sternberg, 2003). The anchor cell appears to use several invadopodia-like protrusions to initially breach the basement membrane, though how this process is initiated remains unclear (Hagedorn et al., 2013). This process is dependent on

integrins and several actin regulatory proteins (Hagedorn et al., 2009). Once the basement membrane is breached, the invasive protrusions are consolidated into one large invadopodium by the netrin receptor, DCC (Hagedorn et al., 2013). This large protrusion physically pushes aside basement membrane locally to widen the breach point for invasion, which demonstrates that mechanical displacement by the cell is an efficient mechanism for removing the basement membrane (Hagedorn et al., 2013). Consistent with this idea, once the anchor cell has crossed the basement membrane, the pore continues to widen further by physical sliding of the basement membrane. Movement and division of the underlying cells could exert traction forces via the *C. elegans* integrin homolog, INA-1/PAT-3 to slide the basement membrane (Ihara et al., 2011). Protease activity has not yet been shown to be directly involved in this system (Kelley et al., 2014), but may be needed in the initial breach of the basement membrane since the matrix metalloprotease, MT1-MMP, is found at the tips of invadopodia in mammalian cancer cells and is required in invasion and degradation of the extracellular matrix (Artym et al., 2006). General protease activity could also potentially partially degrade the entire basement membrane, making it more pliable and allowing the surrounding cells to displace and slide it laterally more easily.

Although proteases are typically thought to be the main mode of breaching the basement membrane, there have been several recent demonstrations of protease-independent breaching; cells instead use mechanical dilation or whole-tissue pressure. In development and throughout the life time of the animal, immune cells travel through the circulatory system patrolling for signs of inflammation (Pflicke and Sixt, 2009). These cells must be able to enter and exit vessels easily to get to sites of inflammation where

there are needed. Interestingly, the basement membrane in lymph vessels is discontinuous, and dendritic cells can enter and exit without the assistance of proteases or integrin mediated adhesion (Pflicke and Sixt, 2009). These discontinuities may be a result of localized decreased deposition of basement membrane, persisting for at least 24 hours and capable of dilating as a cell pushes through (Pflicke and Sixt, 2009).

Another system that has been recently described utilizes mechanical force to breach a weakened basement membrane in mouse embryogenesis. The developing embryo is spatially restricted by the uterus after implantation, inducing elongation and increased mechanical stress at the distal tip of the embryo (Hiramatsu et al., 2013). Decreased collagen IV deposition, but not protease activity, at the distal tip of the embryo thins the basement membrane in combination with this increased pressure, contributes to breaching of the basement membrane (Hiramatsu et al., 2013). The early epiblast cells migrate through these gaps in the basement membrane to establish the distal visceral endoderm (Hiramatsu et al., 2013). The pressure of the whole tissue on the basement membrane and decreased deposition contribute significantly to the rupture of the basement membrane, but dynamic shape and organization changes in the tip cells could also contribute local mechanical forces to facilitate the process of invasion.

Thus cells utilize many strategies for basement membrane remodeling to sculpt tissue morphogenesis. Understanding these reciprocal interactions could provide significant insight into what becomes mis-regulated in disease states. In this thesis, we document how dynamic interactions between the epithelium and basement membrane contribute to overall branching of the embryonic mouse salivary gland. We focus

primarily on mechanical and proteolytic remodeling, finding that they are both required and that they function cooperatively to direct branching of the salivary gland.

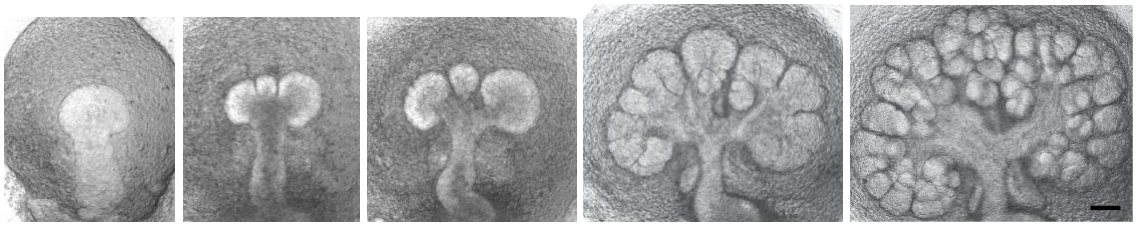

**Figure 1.1. Branching of the mouse salivary gland ex vivo.**

The submandibular gland from an E12 mouse was cultured on a filter floating on media supplemented with vitamin C and tranferrin for 72 hours. Brightfield images were taken at 0, 12, 24, 48, and 72 hours after excision. Glands grown ex vivo mimic the repetitive rounds of epithelial expansion and cleft formation of the gland in vivo, beginning as a single epithelial bud surrounded by a basement membrane and condensed mesenchyme, branching into a highly arborized structure with many buds for secretion of saliva.

# CHAPTER 2

## Epithelial cell dynamics in branching morphogenesis

### Preface

This chapter contains work from our highly collaborative project that was published in *Developmental Dynamics* in 2013 on which I am a co-first author, entitled "Epithelial cell dynamics in branching morphogenesis" (Hsu et al., 2013). Jeff Hsu, Kazue Matsumoto, and the NIDCR gene targeting core generated the homozygous KikGR-expressing mouse line. Jeff Hsu and I designed the experiments, and Andrew Doyle and I carried them out. Hyun Koo tracked cell migration using Volocity, analysis of the results was performed by Jeff Hsu, Andrew Doyle, Kenneth Yamada, and me. Kenneth Yamada and I were the primary authors of the text of the paper. Oversight of the project was provided by my advisor, Kenneth Yamada.

## Introduction

Previous work from our laboratory utilizing GFP-adenovirus infected submandibular salivary glands found that the epithelial cells were highly motile throughout development, and that they became nearly static after birth; these findings suggested this cell motility may be important for morphogenesis of the mouse submandibular gland (Larsen et al., 2006). Although adenovirus was a powerful tool, it penetrated the dense mesenchyme relatively poorly and only randomly infected occasional epithelial cells. A conceptual point of concern about this approach was the possibility that only a certain subpopulation of cells was susceptible to infection and thus labeled for tracking, which could have skewed the results of the motility analysis. Because the mesenchyme was a barrier to infection, mesenchyme-free epithelial rudiments were also used in that previous study for more efficient infection and imaging. This type of culture requires supplementation by several growth factors, including FGF7 and EGF, which could have had stimulatory effects on cell motility. A similar study was subsequently conducted in organoid cultures of the mammary gland (Ewald et al., 2008), and it also suggested that high epithelial motility is important for the development of several branched organs. This latter study, however, had the same potential limitations as the work conducted by our laboratory on the salivary gland.

For these reasons, our laboratory generated a mouse that ubiquitously expressed the photoconvertible Kikume Green-Red (KikGR) protein (Tsutsui et al., 2005) in the cytoplasm. This protein normally fluoresces green, but when exposed to a narrow beam of 405 nm light, the polypeptide backbone is cleaved to irreversibly alter the protein so that it fluoresces red instead of green (Rizzo et al., 2009). This local, light-mediated

photoconversion of small numbers of cells at any location in the gland allowed us to track specific populations of cells within the intact salivary gland, for example comparing those cells in contact with the basement membrane to those surrounded only by other epithelial cells.

## Results

We first confirmed the results of the previous report that the epithelial cells were indeed highly motile and did not migrate collectively as seen in the mammary gland organoids (Ewald et al., 2008; Ewald et al., 2012); instead, the cells moved independently in random patterns. For these experiments, we dissected the salivary glands at E13, cultured the glands overnight, and imaged the following day for 12 hours at 10 minute intervals. We utilized a 405 nm laser controlled by the iLAS system on our spinning disc confocal microscope to photoconvert specific epithelial cells in different regions of the salivary gland to track differences in motility that were based on location. While we could control the size of the region for photoconversion in X-Y very precisely, the 405 nm laser was not confocal. Consequently, we were unable to limit exposure of the sample in the Z-dimension; the result was photoconversion of a column of cells above and below the focal plane. This pattern of photoconversion was not a problem, however, because it allowed us to track multiple cells per bud after each photoconversion, since the cells were highly motile in both X-Y and Z directions.

### *Epithelial cell migration and morphology are region-specific in the salivary gland*

The ability to specifically track small populations of cells in the intact salivary gland allowed us to investigate whether epithelial cells located at different regions within the gland exhibit differences in motility. We tracked cells in three dimensions at three

morphologically distinct regions of the epithelia -- the primary duct, inner bud, and outer bud (Fig. 2.1). The cells in the outer bud region and primary duct contacted the basement membrane, and the inner bud cells were at the center of the bud surrounded only by other epithelial cells. There were substantial differences in both the rates of migration and net displacement of the cells in the different regions (Fig. 2.2). This analysis also highlighted the random individual motility of the salivary gland epithelial cells, which contrasts with several other well-known developmental systems where the epithelia migrate collectively as a sheet in the *Drosophila* egg chamber and during gastrulation, and as groups of cells during neural crest development (Bilder and Haigo, 2012; Kerosuo and Bronner-Fraser, 2012; Nakaya and Sheng, 2009). The outer bud cells were highly motile, migrating an average of 20 μm/hr, which was significantly faster than the inner bud and duct cells that migrated at average rates of 8 and 5 μm/hr, respectively (Fig. 2.3A). The inner cells migrated in relatively circular motions at the middle of the bud, staying very close to the starting point throughout the tracking period (Fig. 2.2B). In comparison, the outer bud cells migrated significantly further than the inner bud cells, often traveling laterally along the basement membrane. Though the migration of the duct cells was calculated to be 5 μm/hr, the cells were almost completely static, translocating only with the overall expansion of the duct as a whole (Fig 2.2A).

The morphology of the cells in the salivary gland epithelial end buds appeared to depend on the proximity of these cells to the basement membrane. Published immunostaining had previously established that the outer-most epithelial cells appear columnar and aligned in orderly fashion along the basement membrane (Onodera et al., 2010; Walker et al., 2008). Photoconversion of only a subset of cells allowed us to

visualize more clearly each individual epithelial cell; the outer bud cells were highly dynamic, frequently extending protrusions and flattening themselves in contact the basement membrane (Fig. 2.4). These outer bud cells were elongated and often migrated laterally along the edge of the basement membrane, frequently bumping up against it (Fig. 2.4B). They exhibited a strong affinity for the basement membrane, leaving the basal boarder only periodically and then immediately returning, often after dividing. The outer cells lost their elongated morphology when they moved away from the basement membrane. In contrast, the internal epithelial cells, particularly those at the center of the end bud, were more rounded and irregularly shaped (Fig. 2.3D). These inner epithelial cells almost never came into contact with the basement membrane and remained confined to the center of the bud. Consequently, the two cell populations within the epithelial bud rarely intermixed.

***Distinct populations of epithelial cells use different modes of migration***

To determine whether this extensive individual cell migration is important for development of the salivary gland, we used inhibitory antibodies and pharmacological inhibitors of proteins integral to the cellular migration machinery, such as integrins and myosin II. Cells interact with the surrounding matrix via integrin attachments, which have been previously shown to be important for branching morphogenesis as a whole (Kadoya et al., 1998; Kadoya and Yamashina, 1993; Kadoya and Yamashina, 2010; Sakai et al., 2003). We hypothesized that the defects in branching after integrin inhibition could have resulted from a defect in cell migration. Inhibitory antibodies to the β1 and α6 integrin subunits were used to inhibit a majority of the cell-basement membrane adhesion in the salivary gland, which resulted in a significant decrease in outer bud cell motility

with no effect on inner bud cell motility (Fig. 2.5). Branching morphogenesis was also significantly impaired as previously reported (Fig 2.6B). Immunostaining revealed a loss of organization of the outer bud cells and aberrant E-cadherin localization to the edge of the cell closest to the basement membrane (Fig. 2.6B). The basement membrane, as visualized by collagen IV, also appeared less condensed and less well-organized. These findings underscore the importance of cell-matrix interactions in branching morphogenesis.

We also investigated the role of non-muscle myosin II in the migration of the salivary gland epithelial cells. Myosin II is a key motor protein in the contractile machinery of the cell, providing mechanical force for cell migration and cell-matrix adhesion maturation (Vicente-Manzanares et al., 2009). Cell migration on 2D surfaces and in 3D matrices is differentially affected by the loss of myosin II: cells on 2D migrate faster and those in 3D migrate slower (Doyle et al., 2009; Even-Ram et al., 2007; Petrie et al., 2012). Actomyosin contraction is also required for morphogenesis of the salivary gland (Fig. 2.6D) and the lung; even though myosin II inhibition initially appeared to increase cleft formation, the clefts did not elongate, resulting in decreased overall branching (Daley et al., 2009; Moore et al., 2005; Plosa et al., 2012). Inhibition of myosin II with the ATPase inhibitor, blebbistatin, decreased the motility of the outer bud cells by more than half, but did not affect the motility of the inner bud cells; these findings were similar to the effect of integrin inhibition on motility (Fig. 2.5). In the salivary gland, myosin II inhibition only affected those cells that contacted the extracellular matrix of the basement membrane, though myosin IIA and B (Fig. 2.7) localize to the cortex of all the epithelial cells of the salivary gland.

Since the inner bud cells did not depend on integrins or myosin II for migration, we next inhibited the protein responsible for cell-cell adhesion, E-cadherin. The cortex of inner bud cells displayed an uninterrupted ring of E-cadherin, in contrast to the outer bud cells, which normally had E-cadherin localized to only three sides of the cell; the edge in contact with the basement membrane lacked any E-cadherin. We found that E-cadherin inhibition had very little effect on the motility of the outer cells, but it did increase the motility of the inner bud cells by more than two-fold (Fig. 2.5). Interestingly, the inhibitory E-cadherin antibody did not have any effect on branching morphogenesis after 20 hours of treatment, even though the inner bud cells were undergoing apoptosis (Walker et al., 2008) during this time, leaving large holes in the middle of the buds (Fig. 2.6C). In contrast, the outer cells were unaffected in their rates of motility and displayed only a slightly less-columnar morphology. However, after 24 hours in the presence of inhibitory E-cadherin antibody, branching slowed, and the size and number of buds were decreased significantly compared to control as previously described (Walker et al., 2008).

**Discussion**

Inhibition of α6/β1 integrin or myosin II decreased only outer cell motility, whereas E-cadherin inhibition decreased only inner cell migration, suggesting that the mode of migration was different in the two populations of cells. Efficient migration of the outer cells was strongly dependent on cell-matrix interaction, indicating that contact with the matrix has a stimulatory effect on the epithelial cells. None of the inhibitory treatments tested accelerated the rate of migration of the outer cells. The inner bud cells were unaffected by the inhibition of the integrins or myosin II. However, their speed of migration was increased after inhibition of E-cadherin, indicating that cell-cell adhesion

restricts the individual motility of the inner bud cells. This finding is consistent with the observed decrease in cell motility as the gland matures and increases its cell-cell adhesions (Hieda et al., 1996; Larsen et al., 2006). Furthermore, both mammary glands and oral epithelial cells lack adherens junctions and tight junctions in early development (Ewald et al., 2008; Hieda et al., 1996; Kadoya and Yamashina, 1993), suggesting that the loss of strong cell-cell attachment to permit high rates of epithelial cell migration is integral to proper development of the glands. Although E-cadherin inhibition slightly decreased the velocity of the outer bud cells, the effect was not nearly as drastic as inhibition of either α6/β1 integrin or myosin II (Fig. 2.5), indicating that the outer cells predominately use a cell-matrix mode of migration. Nevertheless, we have observed cells moving away from the basement membrane and then returning, which suggests that the outer bud cells have the ability to switch quickly these modes of migration.

We speculate that the motility of the outer bud cells may be more integral to the branching of the gland, compared with the inner bud cells since we saw defects in gland morphology only when the migration of the outer cells was decreased. Cleft formation and elongation appeared to occur normally during our 20-hour imaging period in glands that had been treated with the E-cadherin inhibitory antibody, even though the inner bud cells were disrupted and even absent from some regions (Fig. 2.6C). The outer bud cells can migrate inward on the sides of forming clefts, and a decrease in this migration of outer cells into clefts would be expected to slow branching of the gland, which is indeed what we found after their migration was suppressed experimentally by inhibition of either myosin II or integrins (Fig. 2.6B and 2.6D).

The individual, random motility of the epithelial cells could also allow the developing gland to be more plastic and therefore more robust because the gland has the ability to adapt, ameliorating mistakes during development. While there is no standard branching pattern of the salivary gland, unlike the precisely stereotyped pattern of lung branching (Metzger et al., 2008), the gland has some undetermined mechanism to regulate cleft formation such that two clefts do not elongate too close to each other in order to prevent the formation of small, uneven end buds. On the rare occasion that we have observed the formation of more than one cleft, the gland adapted and the two clefts became one (Fig. 2.7); if the outer epithelial cells were not highly motile, this correction would not have been possible. In contrast, the duct exhibited very little morphogenic change over the course of 20 hours, which correlated with very low individual cell motility (Fig. 2.2A). We believe that high cell motility is indicative of plasticity of the tissue and that increased plasticity allows for major changes in tissue architecture during development.

A previous study provided evidence that the outer and inner bud cells are distinct. Even early in development, only the outer epithelial cells express the B1 antigen, a marker characteristic of mature acini, indicating that these outer cells become acini later in development (Walker et al., 2008). In contrast, the inner cells may be more responsible for general proliferation of cells to support and maintain branching, rather than promoting active branching itself. These inner bud cells are destined to become secondary ducts (Walker et al., 2008). These data support the concept that the inner and outer bud cells are physically separate and distinct populations that have different roles during development, and that they help to regulate cell fate after the conclusion of development.

In summary, we used transgenic mice expressing the photoconvertible protein KikGR to analyze single cell migration in the developing salivary gland epithelial bud. This approach was ideal, because it allowed us to track small sub-populations of cells anywhere within the intact gland without the potentially confounding effects of the viral infection approach used previously to track cell motility. We identified two distinct populations of cells in the salivary gland epithelium. One population, termed outer bud cells, consists of cells located at the periphery of the bud that are often in contact with the basement membrane. The cells in the middle of the bud termed inner bud cells are surrounded by other epithelial cells on all sides. We tracked the photoconverted cells in 3D and found that the outer bud cells were highly motile, migrating at an average speed of 20 μm/hr, the inner bud cells were significantly slower at 8 μm/hr, and the duct cells were not migratory, moving only due to overall duct expansion at 5 μm/hr. We found that the high rate of migration of the outer bud cells was dependent on both β1/α6 integrin and myosin II activity. Inhibition of either of these reduced only the motility of outer bud cells and significantly decreased branching morphogenesis. Inhibition of E-cadherin reduced only inner bud cell motility and did not affect branching of the gland over the 20 hour time period we observed. The differences in cell motility and effects of the inhibitors on the different populations of the cells indicated that there are region-specific differences in cell morphology, motility, and fate, which all contribute to different aspects of branching morphogenesis.

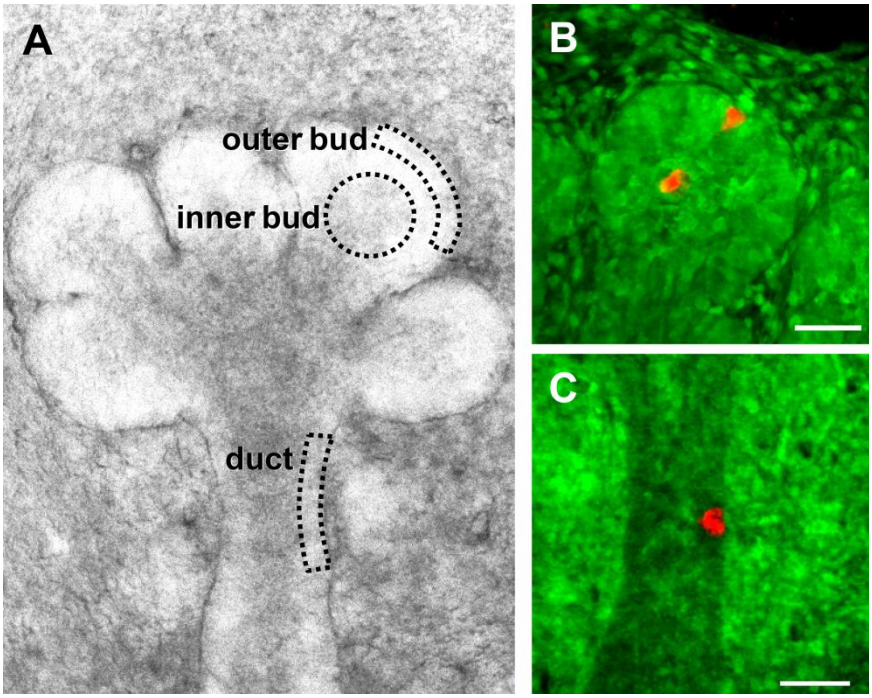


**Figure 2.1. Region-specific florescent highlighting in KikGR salivary gland epithelial cells.**

(A) Brightfield image of an E13.5 submandibular salivary gland indicating the three epithelial regions being compared in this study. The outer bud cells were located at the apex of the bud, away from the clefts. The inner bud cells were located in the center of the bud and the duct cells were on the outer edge of the duct. A focused, narrow beam of 405 nm laser light was used to photoconvert a column of cells from green fluorescence to red in the bud (B) and in the duct (C). Each column of cells contains approximately 8-10 cells. Scale bars are 50 μm.

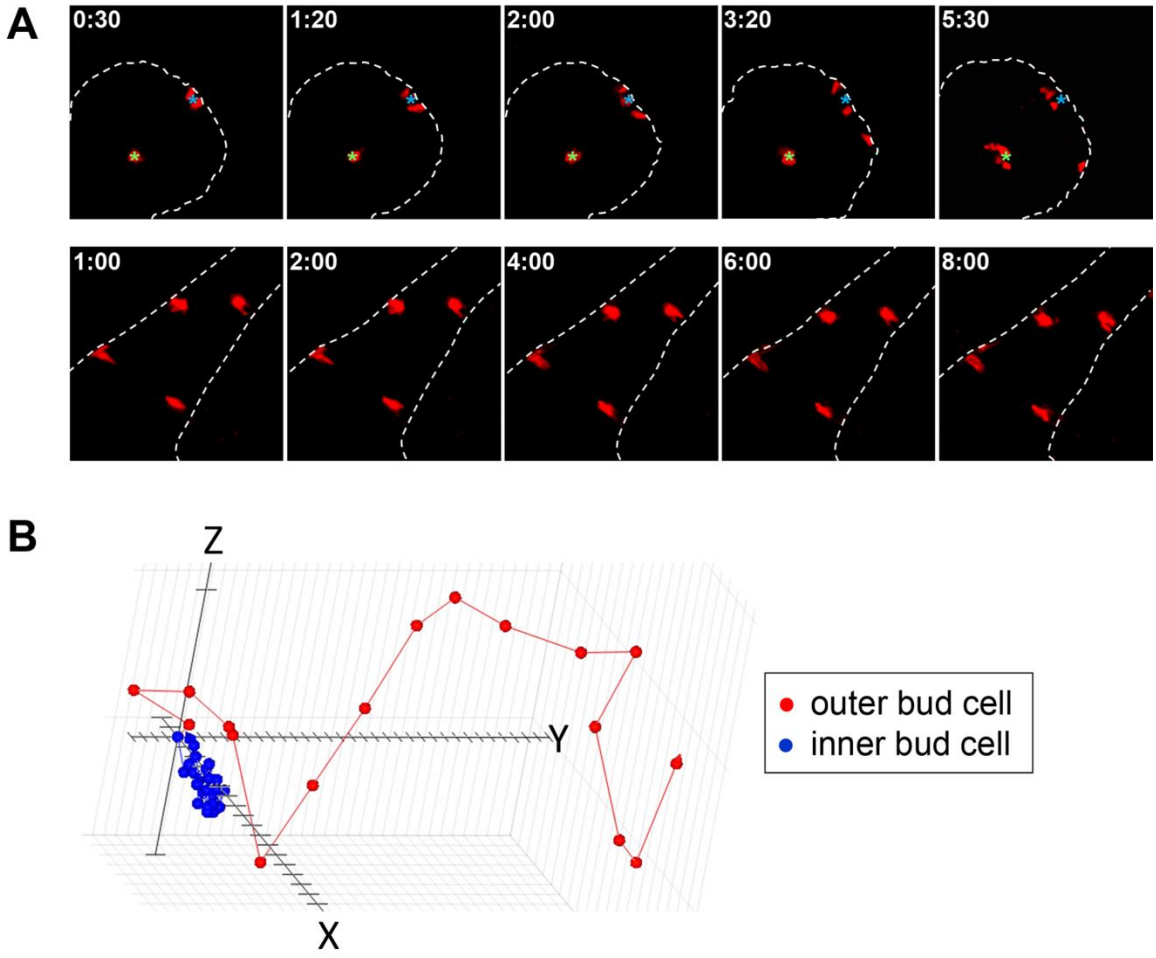


**Figure 2.2. The outer bud cells were highly migratory compared to the inner bud and duct cells.**

(A) Time lapse series of photoconverted KikGR cells in the inner and outer bud cells (top panel) and duct cells (lower panel). In the maximum projection images, the asterisk denotes the starting point of the bud cells and the basement membrane is outlined with white dashed lines. The outer bud cells migrate along the basement membrane much further from their starting point compared to the inner bud cells and the duct cells do not appear to migrate at all. (B) Representative automated 3D computer tracking of an outer cell (red) and an inner cell (blue) using Volocity. The tick marks are spaced 2.5 µm apart on all axes and the time between each point is 10 minutes.

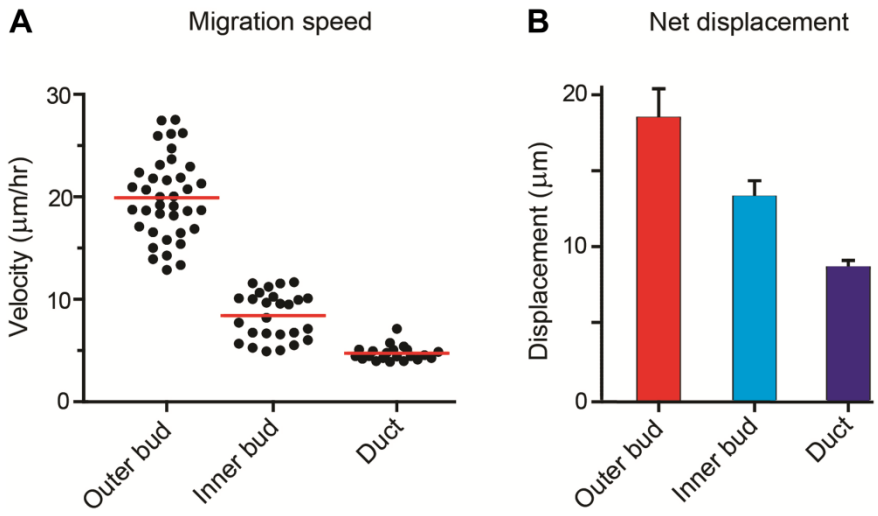


**Figure 2.3. Epithelial cells in different regions of the salivary gland exhibit different velocities.**

(A) Scatter plot analysis of all data points from control glands comparing migration velocities of outer bud cells, inner bud cells, and duct cells. Non-parametric ANOVA analysis and Kruskal-Wallis post-test showed that $p < 0.0001$ for outer vs. inner, outer vs. duct, and inner vs. duct cell velocities. (B) Average net displacement (±SEM) of the outer, inner, and duct cells over 160 minutes; $p < 0.05$ for outer vs. inner bud cells, $p < 0.0001$ for outer vs. duct cells, and $p = 0.011$ for inner vs. duct cells.

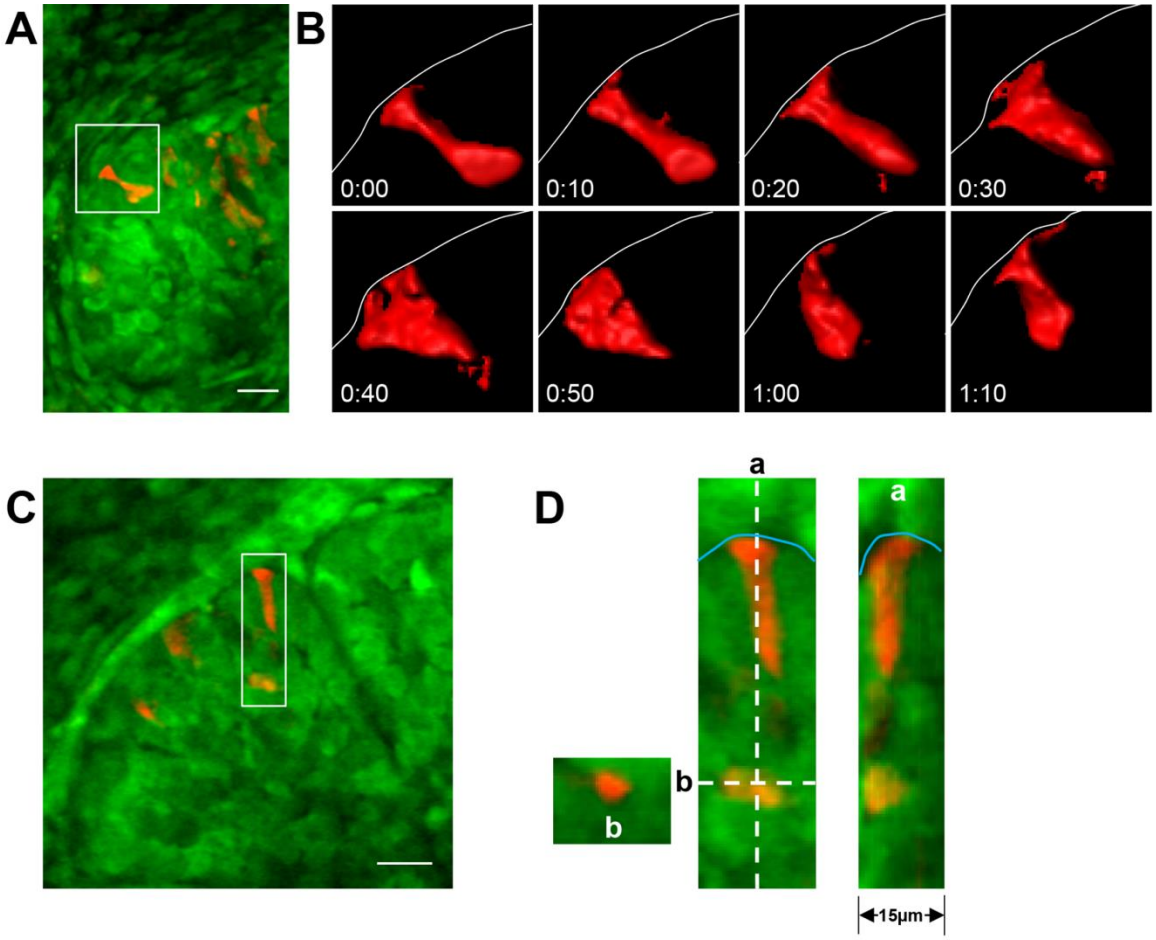


**Figure 2.4. The outer bud cells are highly pleomorphic.**

(A) Low magnification image of photoconverted KikGR cells. An outer bud cell is boxed. (B) Higher magnification image of the boxed outer bud cell with isosurfacing at 10-minute intervals, demonstrating the substantial changes in cell shape while maintaining contact with the basement membrane, outlined in white. (C) Low magnification image of photoconverted KikGR cells with an outer cell and inner cell boxed. (D) Orthogonal views of the boxed cells from (C), on three axes with the basement membrane outlined in cyan. The inner bud cells are small and rounded compared to the elongated outer bud cells. Scale bars are 20 µm.

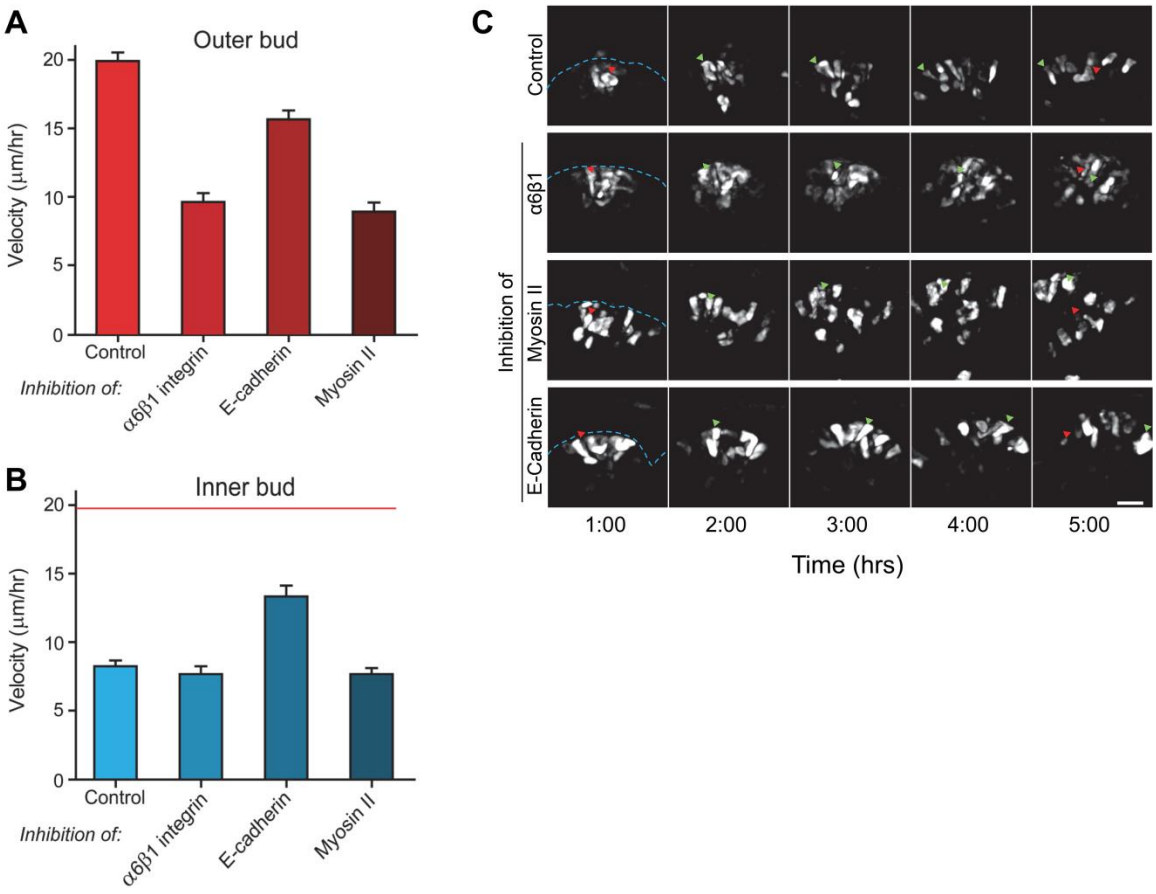


**Figure 2.5. Changes in the velocities of regional cell migration with the addition of various inhibitors.**

(A) Average rates of outer bud cell migration (±SEM) in glands treated with a combination of α6 and β1 inhibitory antibodies at 100 mg/ml each, 100 mg/ml E-cadherin inhibitory antibody, or 50 µM blebbistatin which inhibits all non-muscle myosin II isoforms. In comparison, (B) average rates of inner bud cell migration (±SEM) with the same inhibitors. The red line at the top of the graph represents the average speed of migration for the control outer bud cells. (C) A 4-hour timelapse series of the movement of the outer bud cells with the previously mentioned inhibitors. The red arrowheads indicate the starting position of the cell and the green arrowheads indicate the position of

the cell at the current time point. The basement membrane is shown at the first time point traced in cyan; scale bar is 20 μm.

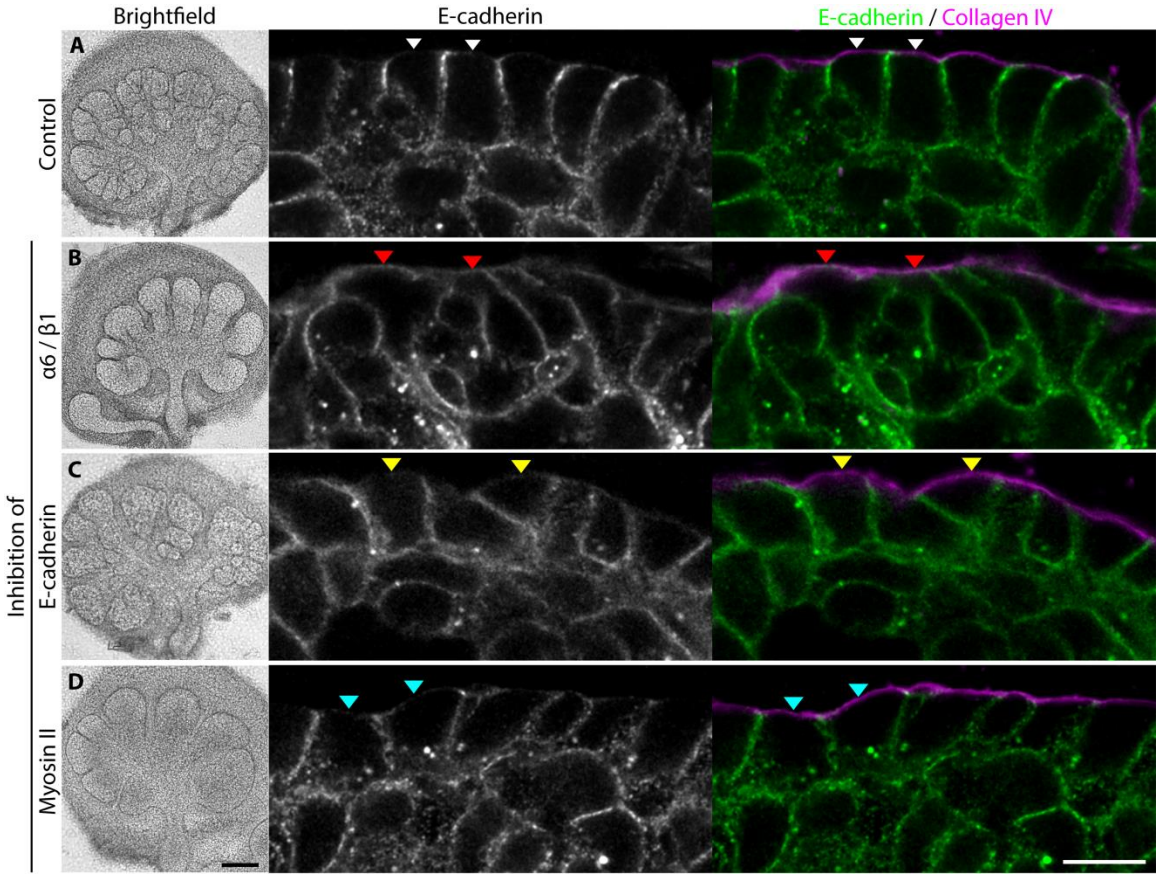


**Figure 2.6. Salivary gland morphological changes with various inhibitors.**

Salivary glands at E14 after being treated with no inhibitor (A), a mixture of (Ha2/5) β1 and (GoH3) α6 inhibitory integrin antibodies at 100 mg/ml each (B), 100 mg/ml inhibitory (ECCD-1) E-cadherin antibody (C), or 50 μM blebbistatin (D) for 10 hours. Brightfield images on the left show the overall gland morphology after treatment; scale bar is 200 μm. The middle panel shows cell shape via E-cadherin staining, colored arrowheads show no E-cadherin localization at the apical basement membrane in A, C, and D, and abnormal localization in B. Overlay images on the right show the basement membrane in magenta and E-cadherin in green; scale bar is 10μm.

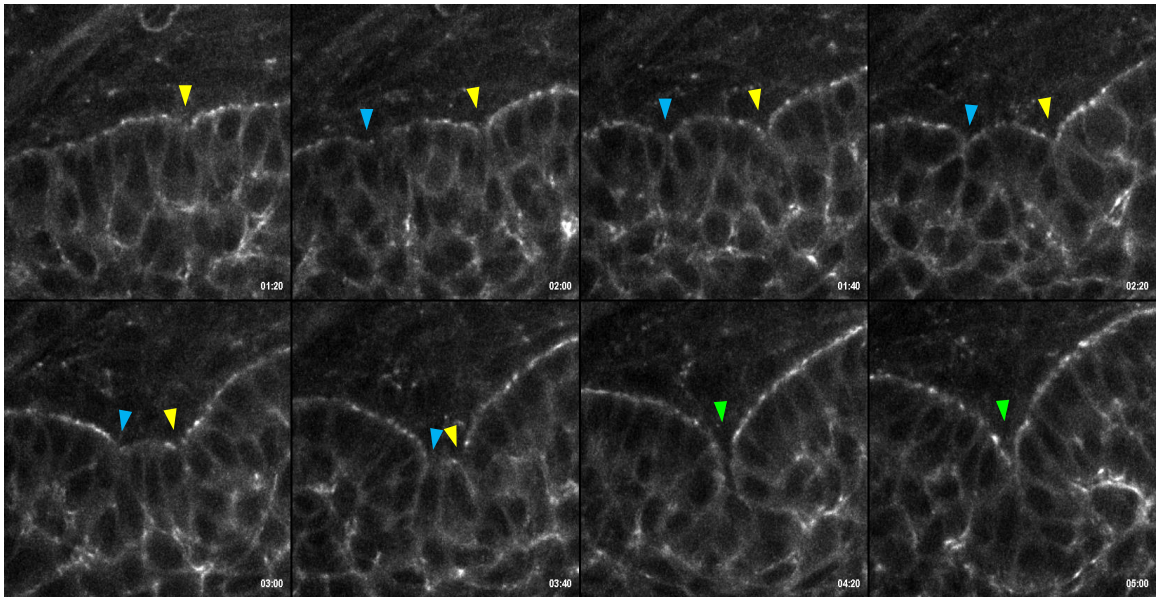


**Figure 2.7. The developing salivary gland is easily adaptable.**

The above are images taken at 40-minute intervals from a timelapse series of a GFP-myosin IIB salivary gland at E13 undergoing cleft formation. Initially two clefts formed (blue and yellow arrowheads) and as they elongated the two clefts joined to become one (green arrowhead), demonstrating the adaptability of the developing salivary gland. Typically a single cleft initiates and elongates.

# CHAPTER 3

## Basement membrane remodeling and dynamics allows epithelial expansion during branching morphogenesis

### Preface

The epithelial cells are highly motile, as we described in the previous chapter, and yet they stay confined within the basement membrane all throughout development. The basement membrane serves as an important physical barrier between the epithelium and mesenchyme compartments, which is particularly important when the epithelial cells are so migratory to prevent tissue mixing. We discuss the role of basement membranes in epithelial expansion this chapter.

For this third chapter, I have adapted parts of my first author paper entitled, "Local and global dynamics of the basement membrane during branching morphogenesis require protease activity and actomyosin contractility" that has been submitted and is under review at the journal, *Developmental Biology*. Andrew Doyle provided expertise for the rapid imaging of the epithelial protrusions and my advisor, Kenneth Yamada supervised the work.

## Introduction

Normal embryonic development requires expansion of epithelial tissues within a basement membrane, which is a stiff, sheet-like type of extracellular matrix. Rapid expansion of epithelia occurs during specific stages of branching morphogenesis of lung, submandibular salivary gland, kidney, mammary gland, and other organs. This process of epithelial bud expansion and branching by cleft formation is a key developmental process to maximize organ epithelial surface area for secretion and adsorption. Although the morphology of these embryonic organs differs (Fig. 1A), all such epithelia are encapsulated by a basement membrane that separates the epithelium from the surrounding stroma containing mesenchyme cells (Andrew and Ewald, 2010; Daley and Yamada, 2013; Kim and Nelson, 2012). Basement membranes play multiple important roles in morphogenesis, with functions that include providing tissue structural support and boundaries, mediating growth factor signaling, and providing polarity cues (Rozario and DeSimone, 2010). Recent studies in *Drosophila* egg chamber, mammary and salivary glands have shown that cells can orient, translocate, and accumulate the surrounding basement membrane to help shape the architecture of the tissue (Daley and Yamada, 2013; Fata et al., 2004; Haigo and Bilder, 2011; Larsen et al., 2006). Proteolytic remodeling of the basement membrane is required for branching morphogenesis in several organs (Banerjee et al., 1977; Nakanishi et al., 1986; Wessells and Cohen, 1968). Specifically, matrix metalloproteases are necessary for lung, salivary and mammary gland branching, allowing outgrowth (Fata et al., 2004; Oblander et al., 2005) and growth factor release (Rebustini et al., 2009) contributing to branching.

Both the epithelial and mesenchymal cell populations of branching organs can be surprisingly motile during development (Ewald et al., 2008; Larsen et al., 2006; Metzger and Krasnow, 1999; Shakya et al., 2005). In the salivary gland, motility rates of epithelial cells immediately adjacent to the basement membrane can be even higher than in the interior of the buds, with cells migrating at average rates of 20 μm/hr (Hsu et al., 2013). This high rate of epithelial cell motility relies on integrin-dependent interactions with the basement membrane (Hsu et al., 2013). The substantial motility of the epithelial cells during early development underscores the importance of maintaining the basement membrane as a barrier to prevent intermixing of epithelial and mesenchymal cell compartments to permit normal morphogenesis. While many laboratories have investigated how cells invade through a basement membrane, particularly in pathological processes such as cancer metastasis (Rowe and Weiss, 2009), the fundamental question of how normal embryonic epithelia can expand rapidly while remaining enclosed by a basement membrane is poorly understood.

## Results

### *The basement membrane surrounding several embryonic branched organs is perforated*

During branching of the lung, mammary gland, and salivary gland, the basement membrane is known to become thinner or to display increased remodeling at the tips of expanding epithelial buds compared to cleft and duct areas (Bernfield and Banerjee, 1982; Fata et al., 2004; Mollard and Dziadek, 1998; Silberstein and Daniel, 1982); these findings suggest that these regions of basement membrane might exhibit increased mechanical compliance or distensibility (Moore et al., 2005) that could permit local tissue

expansion and guide branching behavior. To determine if the basement membrane demonstrates local morphological and structural changes in these regions consistent with this hypothesis, we examined the basement membrane surrounding the end buds of salivary glands, lungs, and kidneys undergoing morphogenesis at stages of rapid expansion (Fig. 3.1A). By imaging using confocal microscopy and creating maximum-intensity projection images of organs immunostained for collagen IV, the characteristic structural collagen of basement membrane, as well as the glycoprotein laminin, revealed that the basement membrane was not uniform, but was instead perforated by numerous well-defined microscopic holes (Fig. 3.1B, 3.1C, 3.1D). The micro-perforations, or holes, were most prominent at regions of the basement membrane surrounding the tips of the expanding end buds and were absent from the cleft and duct areas where expansion was low (Fig. 3.1B).

***The micro-perforations span the entire basement membrane***

Focusing on developing salivary glands, we found that the holes appeared to penetrate through the entire basement membrane according to immunolocalization of three major constituents of basement membrane, collagen IV, laminin, and perlecan, a heparan sulfate proteoglycan (Yurchenco, 2011). A micro-perforation observed for each of these components could be matched exactly with a corresponding perforation involving each of the other two components (Fig. 3.2A). In single-plane, 0.38 μm optical Z-sections of the bud, the basement membrane appears physically thinner at the tip compared to the base of the cleft (Fig. 3.2B), consistent with previously published results.

We obtained complementary evidence for numerous microscopic holes spanning the basement membrane by live-organ imaging of cellular extensions. Basal epithelial

cells were frequently found to extend cell surface protrusions through and beyond the basement membrane holes (Fig. 3.2C); these bleb-like protrusions could extend as far as 5 μm beyond the basement membrane. These numerous protrusions were highly dynamic and often extended repetitively through the same hole, confirming patency of the micro-perforations. These membrane protrusions were observed only at the tips of end buds, protruding through basement membrane perforations in both embryonic salivary gland and lung.

***Basement membrane micro-perforation occurs while the tissue is rapidly expanding***

The presence of micro-perforations in the basement membrane was associated with the stage of embryonic salivary gland development with the highest epithelial expansion and outgrowth (Fig. 3.3). We found that at E12.5, when the salivary gland is a single epithelial bud, the basement membrane had no perforations. At E13.5, when the gland was undergoing massive branching and epithelial expansion, the number and size of perforations reached their peak. At E14.5, when branching had slowed significantly and differentiation begins, the basement membrane appeared relatively smooth and free of perforations, as it does in the post-natal gland.

We quantified the basement membrane micro-perforations in developing salivary glands. The sizes of the holes varied enormously, with the cross-sectional area of a perforation ranging from 0.01 to 15 $\mu m^2$, though > 90% of the perforations had areas < 5 $\mu m^2$; their overall average area was 1.6 $\mu m^2$ ± 2.1 (standard deviation). This area is substantially smaller than an epithelial cell (estimated as ~25 $\mu m^2$ at the basal surface) and would keep the epithelium compartmentalized from the mesenchyme. We found that the distribution of the perforations varied across the end bud (Fig. 3.4A); the highest

density was near the tip (Fig. 3.4B) where 27% of the basement membrane surface area was lost to holes. In terms of frequency, at the tip of the bud, there was an average of 60 holes per 500 $\mu m^2$ or 3 perforations per cell (Fig. 3.4C). This number fell to only ~1 hole per cell toward the middle (equator) of the bud. The percent perforated area decreased dramatically closer to the center of the bud by almost 7-fold, as the number and size of the perforations decreased (Fig. 3.4C, 3.4D), so that the basement membrane was 94% intact near the center of the bud. The increased concentration of large basement membrane perforations near the tips of the end buds could potentially increase basement membrane flexibility to permit epithelial expansion.

***Extensive perforation of the basement membrane increases its distensibility***

To determine whether this extensive micro-perforation alters the mechanical flexibility or distensibility of the basement membrane, regions of E13 salivary glands were imaged live in the presence of fluorescently labeled, non-perturbing collagen IV antibody. We found the basement membrane to be highly dynamic (Fig. 3.5). Epithelial cells appeared to continuously "tug" on the matrix such that the micro-perforations frequently changed shape and size; the area of an individual perforation could fluctuate as rapidly as 4 $\mu m^2$ in less than 1 minute (Fig. 3.5A). We found that the repetitive dilation and contraction of the micro-perforations was due to rapid physical distortion of the basement membrane, rather than degradation or deposition of basement membrane, since the fluctuations stopped within minutes of addition of the myosin II ATPase inhibitor, blebbistatin (Fig. 3.5A). The fact that the basement membrane was so readily deformed indicated that the basement membrane was highly compliant.

An additional method for evaluating basement membrane extensibility was to measure stretching of the basement membrane itself. We tracked pairs of fiduciary marks on the basement membrane surface and found distensibility, defined as the maximum distance between two points subtracted from the minimum distance within a 20 minute time period, was 2-fold higher near bud tips compared to the center of the bud (Fig. 3.5B, 3.5C). There was greater basement membrane stretching in the area of the gland with larger, more numerous basement membrane micro-perforations and high tissue expansion, a finding consistent with enhanced local basement membrane flexibility due to the perforations. The distensibility of the basement membrane was dependent on actomyosin contraction, since these basement membrane dynamics were inhibited by the addition of blebbistatin (Fig. 3.5A).

***Both protease activity and myosin II contractility are required for perforation formation and maintenance***

A specific protease produced by the epithelium, MT2-MMP, had been previously implicated in releasing growth factors from the basement membrane that promote epithelial proliferation (Rebustini et al., 2009). We hypothesized that additional protease activity would be needed to form the basement membrane perforations, which required the parallel loss of a collagen, a glycoprotein, and a proteoglycan. We tested this by treating the glands at E12.5, prior to basement membrane perforation formation, with a variety of protease inhibitors. The most effective was the broadest protease inhibitor, batimastat (BB-94). With this inhibitor, micro-perforations did not form and branching was significantly inhibited (Fig. 3.6A, 3.6B). Protease activity was also required for maintenance of the perforations; treatment of the glands with BB-94 at E13, when perforations were already present, resulted in shrinking and disappearance of the micro-

perforations within four hours (Fig. 3.6C). Treatment with a slightly less broad protease inhibitor, GM6001 (Fig. 3.6C), had similar effects, to a lesser degree compared to glands treated with BB-94; tissue inhibitors of metalloproteases (TIMPs) had no effect (Fig. 3.6D). These data suggest that multiple proteases are involved in forming and maintaining basement membrane perforations.

Immunostaining for collagen IV in glands treated with the protease inhibitor BB-94 revealed enhanced basement membrane accumulation around the end buds (Fig. 3.6B), consistent with reversal of protease-mediated degradation of the basement membrane. Live-organ imaging revealed that treatment of salivary glands with BB-94 gradually inhibited basement membrane motion; after 12 hours, perforations were substantially diminished, collagen IV increased three-fold around the end buds (Fig. 3.7C), and distensibility was significantly reduced (Fig. 3.5B). Additionally, kymograph analysis (Fig. 3.7B) of this 12-hour time period revealed a two-fold reduced rate of bud outgrowth after prolonged protease inhibition (Fig. 3.7D). Although branching morphogenesis was strongly inhibited, this decreased expansion was not accompanied by altered cell proliferation as determined by EdU incorporation (Fig. 3.7E). These findings suggest that the accumulation and stiffening of basement membrane around the end buds after protease inhibition restricted expansion of the end buds and inhibited normal branching morphogenesis of the gland.

Because a particularly striking feature of basement membrane behavior was reduced mobility after myosin II inhibition with a rapid cessation of the mechanical tugging on the basement membrane (Fig. 3.5A, 3.5B), we examined whether actomyosin contractility had a role in the formation and maintenance of basement membrane micro-

perforations. Myosin IIA and IIB were found to be enriched at the epithelial cell cortex adjacent to the basement membrane (Fig. 3.8A). At E12.5, treatment with blebbistatin inhibited cleft progression and prevented micro-perforation formation (Fig. 3.8B, 3.8C). At E13.5, accompanying the loss of basement membrane dynamics, the size and numbers of perforations decreased progressively and were absent within four hours following treatment (Fig. 3.6C). Another inhibitor of actomyosin contraction, Y27632, had similar inhibitory effects on the basement membrane perforations (Fig. 3.6C). Combining treatment with blebbistatin and BB-94 accelerated closure of the basement membrane holes by two-fold (Fig. 3.8D), suggesting that the proteases and myosin II function in distinct, yet cooperative, ways to maintain the micro-perforations. Consequently, both broad protease activity and myosin II-mediated mechanical force are required for generating and maintaining regional basement membrane perforations and successful epithelial expansion.

**Discussion**

The basement membrane can be breached by migrating cells at specific stages of development in events involving mass outward movements of cells or local invasion by embryonic or tumor cells (Rowe and Weiss, 2008). This study addresses an alternative form of tissue remodeling in which motile epithelial cells and tissues expand rapidly during tissue morphogenesis while still remaining fully confined by a basement membrane barrier. This process allows for continued exposure of the epithelial cells to polarity cues and adhesive/signaling substrates while preventing tissue intermixing.

Our novel findings include the following: (1) the basement membrane becomes perforated by hundreds of microscopic holes during rapid expansion of developing buds

of salivary glands, lung, and kidney; (2) these micro-perforations are most numerous at the tips of buds where expansion is most rapid; (3) they appear at the developmental stage associated with high outward epithelial expansion; (4) these holes provide sites for epithelial cell protrusion through the basement membrane that extend out into the mesenchyme; (5) these micro-perforations and the basement membrane as a whole undergo rapid stretching movements that are myosin II-dependent and indicative of basement membrane flexibility; and (6) formation and maintenance of these perforations, as well as rapid tissue expansion, require contributions from both broad protease activity and myosin II contractility.

Our study was able to document the existence of numerous micro-perforations by combining single-plane confocal optical slices into maximum-intensity projections to visualize the basement membrane as a whole, rather than as tissue cross-sections. Interestingly, the overall thickness of the basement membrane is not obviously different in comparisons of the tip and the sides of salivary gland buds; instead, the micro-perforations produced a lace-like pattern toward the tips (Fig. 3.1B, 3.2B). Therefore, in this particular developmental system, simple thinning of the basement membrane alone does not seem to provide increased compliance, and its increased flexibility is instead associated with the presence of the micro-perforations. In striking contrast, the basement membrane is thicker and more abundant at the base of the broadening clefts that delineate the secondary duct. In fact, previous research had suggested the importance of extracellular matrix accumulation, especially collagen, in this region to stabilize the clefts and ultimately sculpt the tissue (Banerjee et al., 1977; Fukuda et al., 1988; Grobstein and Cohen, 1965). There are now multiple examples of key roles of extracellular matrix

interactions affecting tissue architecture and specific movements (Daley and Yamada, 2013). In some cases, oriented matrix fibrils can direct tissue movements or rotation (Tanner et al., 2012; Wang et al., 2013), which contrasts with the process we describe involving a flat, sheet-like basement membrane barrier.

Published ultrastructural data support the existence of these micro-perforations and cell protrusions: a series of thin-section electron microscopy studies in the 1970's of epithelial-mesenchymal inductive interactions in embryonic tissues identified single cellular protrusions through a discontinuity in the basement membrane during the development of lung, kidney, salivary gland, and tooth (Bluemink et al., 1976; Cutler and Chaudhry, 1973; Lehtonen, 1975; Slavkin and Bringas, 1976). In these studies the cellular protrusions and basement membrane breaks occurred primarily at the tips of the epithelial buds but the authors did not comment on the frequency of such events. Our whole-mount immunofluorescence data demonstrate remarkably large numbers of such gaps or perforations in the basement membrane with multiple, highly dynamic epithelial protrusions that can extend up to 5 μm into the mesenchymal cell compartment. Our characterization of their dynamics indicates that these protrusions periodically fill the perforations, maintaining patency; in fact, we speculate that they might contribute to helping expand the perforations. The edges of perforations expand and contract rapidly and often repetitively, and this process is blocked by inhibition of actomyosin contractility with the myosin II inhibitor blebbistatin; the perforations ultimately close after this inhibition. These findings identify a mechanical role for myosin II in maintaining the micro-perforations. Interestingly, recently published data indicate that

mechanical forces can play an additional role in the process of traversing the basement membrane by invading cells (Hagedorn et al., 2013; Hiramatsu et al., 2013).

We suggest that the micro-perforations may also contribute to epithelial-mesenchymal signaling by diffusible molecules, in addition to direct contact; specifically, growth factors such as FGFs (Patel et al., 2006) might diffuse more readily through these ~2 $\mu m^2$ gaps rather than binding to the basement membrane (Patel et al., 2007). Additional growth factors are likely released as the cells degrade the matrix to form the micro-perforations contributing to epithelial proliferation and overall branching morphogenesis (Ortega and Werb, 2002; Rebustini et al., 2009). Consequently, the hundreds of micro-perforations per bud may play multiple roles in development by permitting trans-tissue contacts, increasing diffusion/release of key growth factors, and enhancing basement membrane flexibility to permit overall tissue expansion.

This new developmental process involving multiple microscopic perforations in an otherwise intact basement membrane to preserve the integrity of an epithelial tissue contrasts with processes such as gastrulation and neural crest migration in which the basement membrane fragments to permit mass emigration of cells from the ectoderm or neural tube (Kerosuo and Bronner-Fraser, 2012; Nakaya and Sheng, 2009). It also contrasts with single-cell invasion by tumor cells or anchor cells in *C. elegans*, which locally degrade the basement membrane through a hole that enlarges until the cell can traverse this barrier (Kelley et al., 2014). During branching morphogenesis, however, the highly dynamic epithelial tissue must remain constrained within a sheet-like basement membrane while expanding. Although the dynamic epithelial protrusions we documented were large at times (up to 5 μm long) they never resulted in crossing of the basement

membrane by the cell body, even though the holes were often distorted substantially by myosin II-dependent contractions. We speculate that exaggerated activity of proteases and actomyosin contractility might allow whole-cell invasion. In conclusion, extensive micro-perforation at regions of rapid expansion in a developing organ provides an elegant solution to the problem of how to permit controlled, directional outgrowth of a tissue while still encapsulating motile individual cells during morphogenesis.

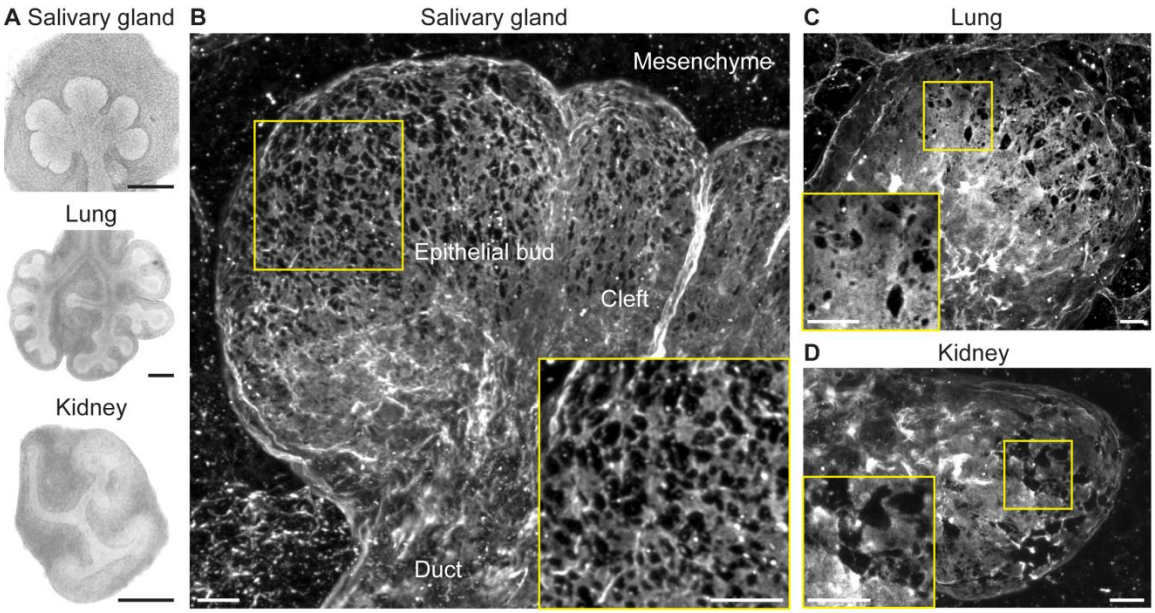


**Figure 3.1. Micro-perforated basement membranes are present in multiple embryonic organs.**

(A) Brightfield images of an E13 salivary gland, E11 lung, and E11 kidney show the differences in morphology among developing branched organs; scale bars are 200 μm. (B) Maximum-intensity projection of an E13 submandibular salivary gland immunostained for collagen IV with labels indicating an epithelial bud with a developing cleft and its duct, surrounded by mesenchyme. Maximum projection images of confocal slices of E11 lung (C) and kidney (D) immunostained for laminin. Scale bars are 20 μm and 10 μm for the insets.

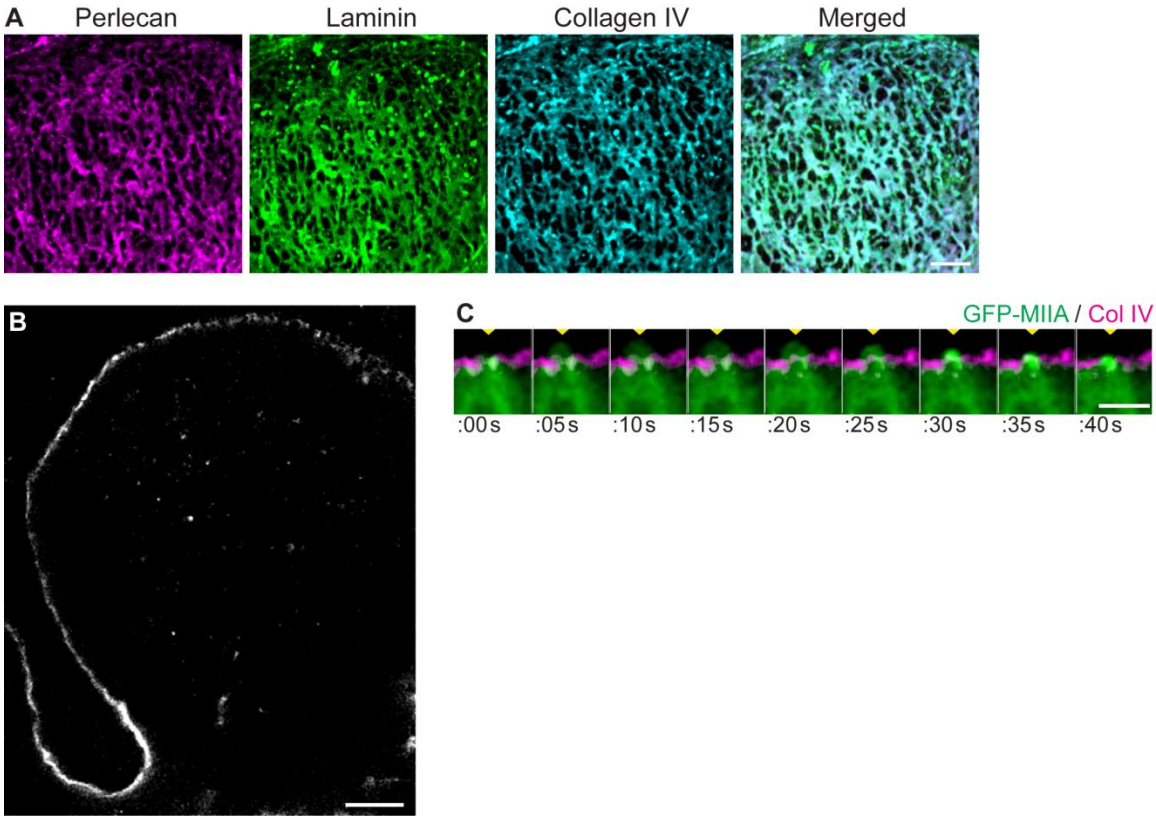


**Figure 3.2. Micro-perforations penetrate through the entire basement membrane.**

(A) Maximum projection images of an E13 submandibular salivary gland stained for several basement membrane (BM) components- perlecan (magenta), laminin (green), collagen IV (cyan) and merged; scale bar is 10 μm. (B) Single Z-slice through an E13 salivary gland stained for collagen IV; scale bar is 20 μm. (C) 40-second montage of a basal epithelial cell from an E13 GFP-myosin IIA gland (green) showing a cell process protruding (yellow arrowheads) through the basement membrane (magenta) imaged with fluorescently tagged collagen IV antibody; scale bar is 5 μm.

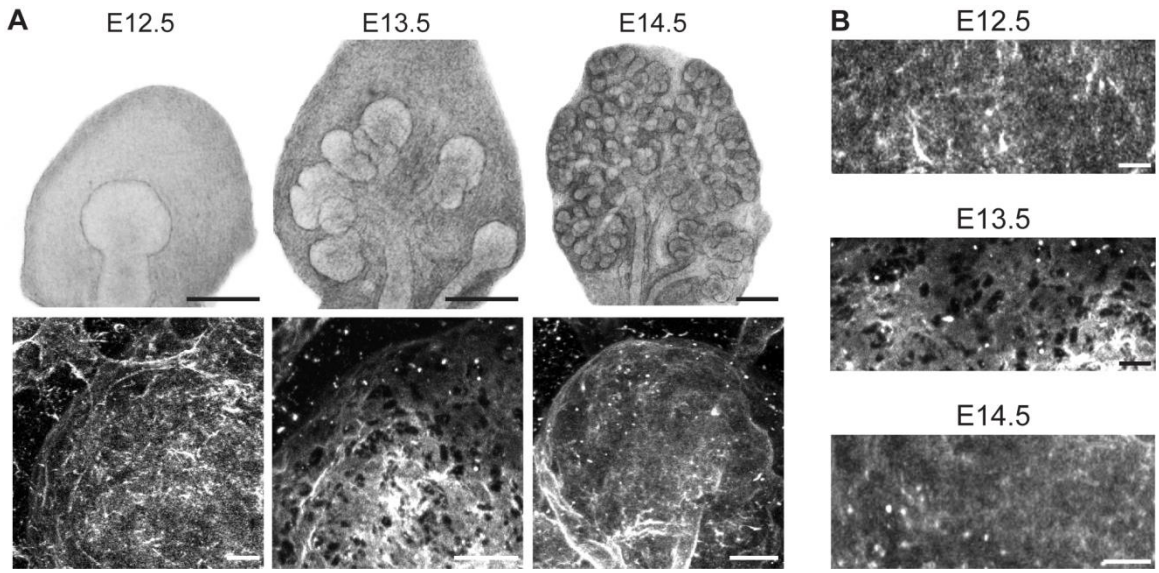


**Figure 3.3. Basement membrane holes are associated with specific developmental stages.**

(A) Brightfield and collagen IV maximum projection images of glands dissected at E12.5, E13.5 or E14.5. Brightfield scale bar is 100 μm and collagen IV scale bar is 10 μm. (B) Enlarged maximum projection images of collagen IV immunostaining of salivary glands at E12.5, E13.5, and E14.5; scale bars are 5 μm.

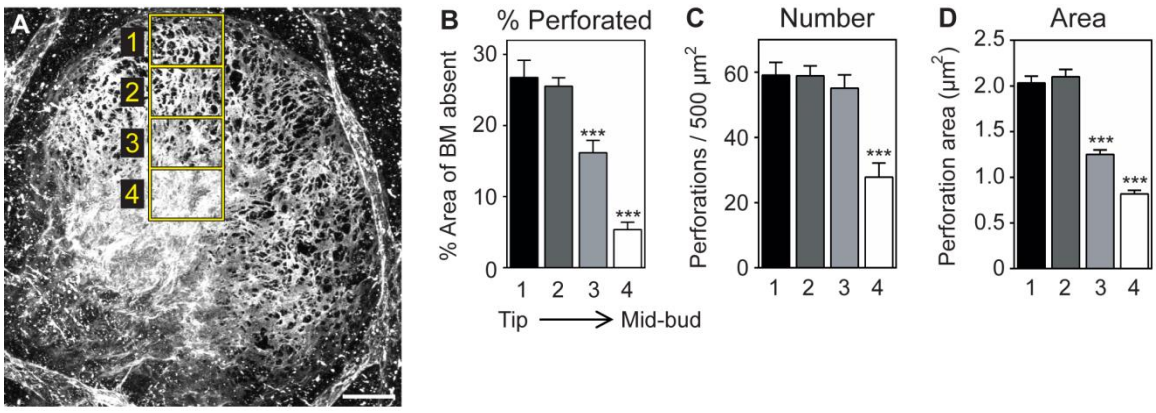


**Figure 3.4. Characterization of basement membrane micro-perforations.**

(A) Maximum projection of E13.5 salivary gland stained for collagen IV marked with 4 rectangular regions of equal size, starting at the tip of the bud and ending at the center of the bud, utilized for comparative analysis; scale bar is 20 µm. (B) Average percent surface area of basement membrane absent (±SEM) based on region: region 1 = tip of the bud and 4 = center of the bud, as shown in 2B. (C) Average number of holes per 500 µm area of basement membrane and (D) average perforation areas (±SEM) of each of the 4 different regions of the bud. (n= 4 experiments, 10 glands), ***$p<0.001$, ANOVA, Tukey post-test compared to region 1.

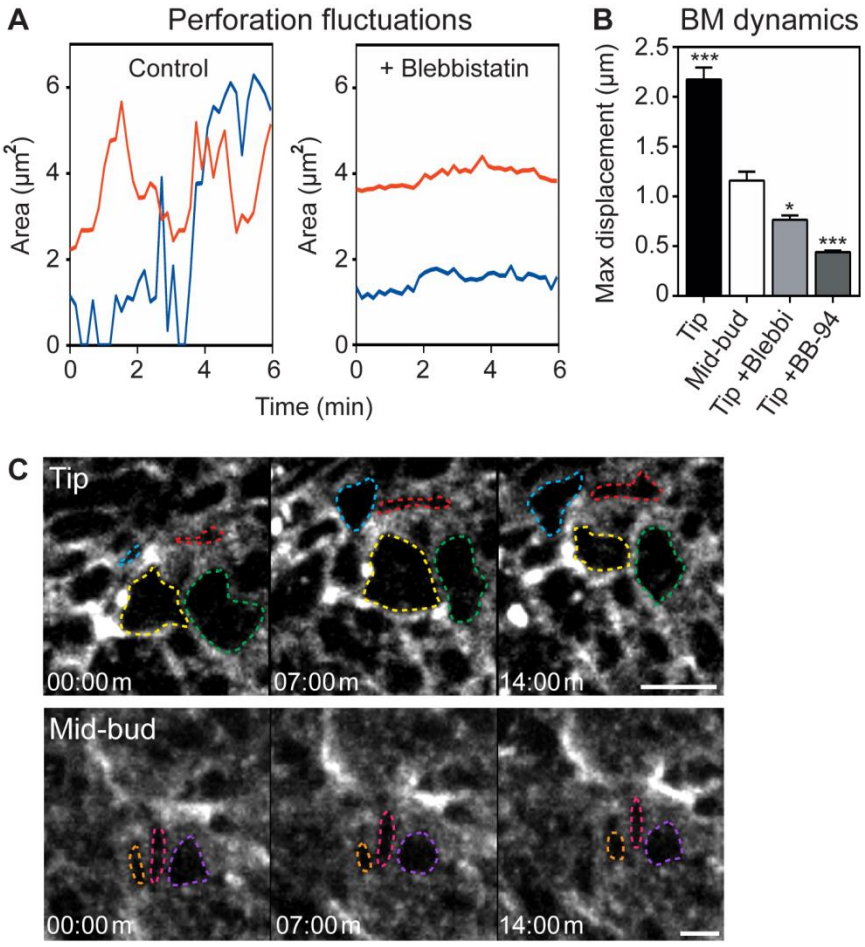


**Figure 3.5. Micro-perforations increase basement membrane distensibility.**

(A) Change in area of two example holes in control and 50 μM blebbistatin-treated glands imaged over a span of 6 minutes. (B) Average distensibility of the basement membrane (±SEM) expressed as maximum displacements of fiduciary marks within a 20-minute assay period comparing a region near the tip versus mid-bud, and at the tip of glands treated with 50 μM blebbistatin or 5 μM BB-94. ($n \geq 4$ experiments, 8 glands), *$p<0.05$, ***$p<0.001$, ANOVA, Tukey post-test compared to mid-bud. (C) Tracking of (color-coded) perforations over 14 minutes at the tip and mid-bud regions of an E13 salivary gland; scale bar is 5 μm.

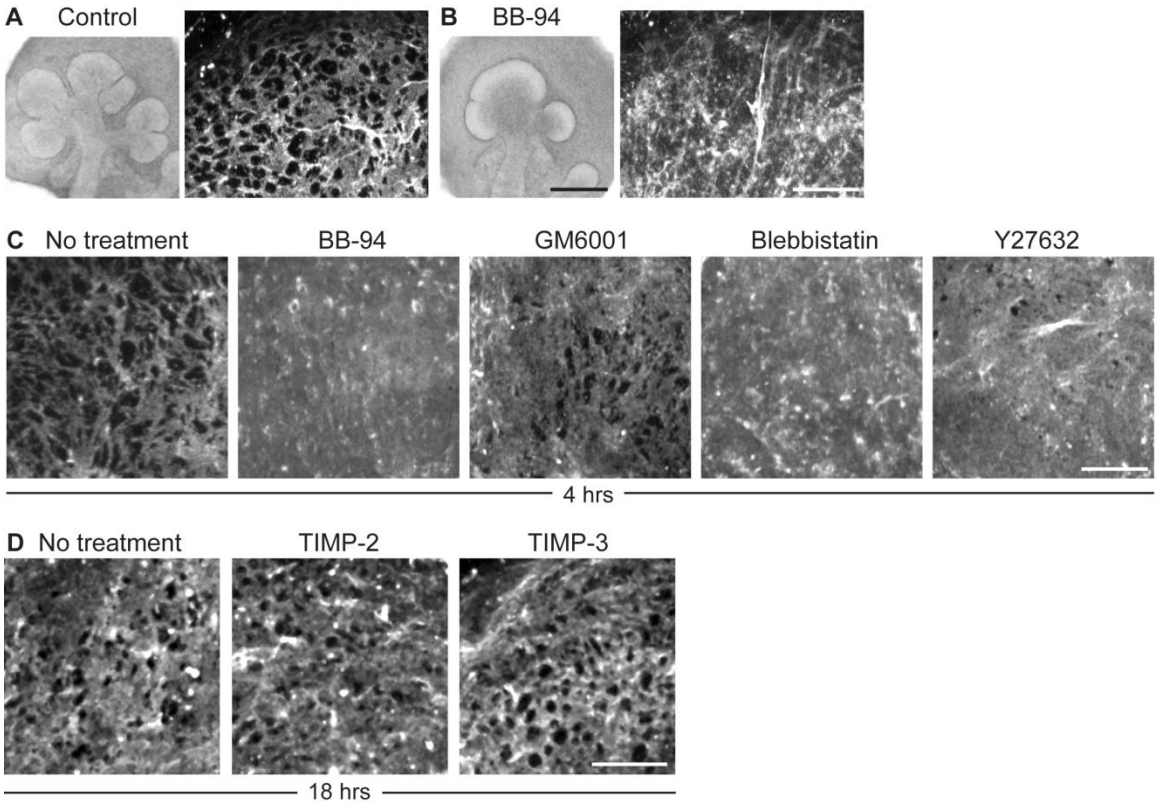


**Figure 3.6. Formation and maintenance of basement membrane micro-perforations require protease activity.**

(A) Control and (B) 5 μM BB-94 treated E12.5 glands immunostained with collagen IV after 24 hours. Brightfield scale bar is 200 μm and collagen IV scale bar is 10 μm. (B) Maximum projection images of E13 submandibular salivary glands with no treatment, treated with broad protease inhibitors (5 μM BB-94 or 25 μM GM6001), or inhibitors of actomyosin contractility (50 μM blebbistatin or 20 μM Y27632) for 4 hours then immunostained for laminin; scale bar is 10 μm. (C) Maximum projection images of E13 salivary glands with no treatment, treated with 4 μg/mL of recombinant TIMP-2 or TIMP-3 overnight and immunostained for collagen IV; scale bar is 10 μm.

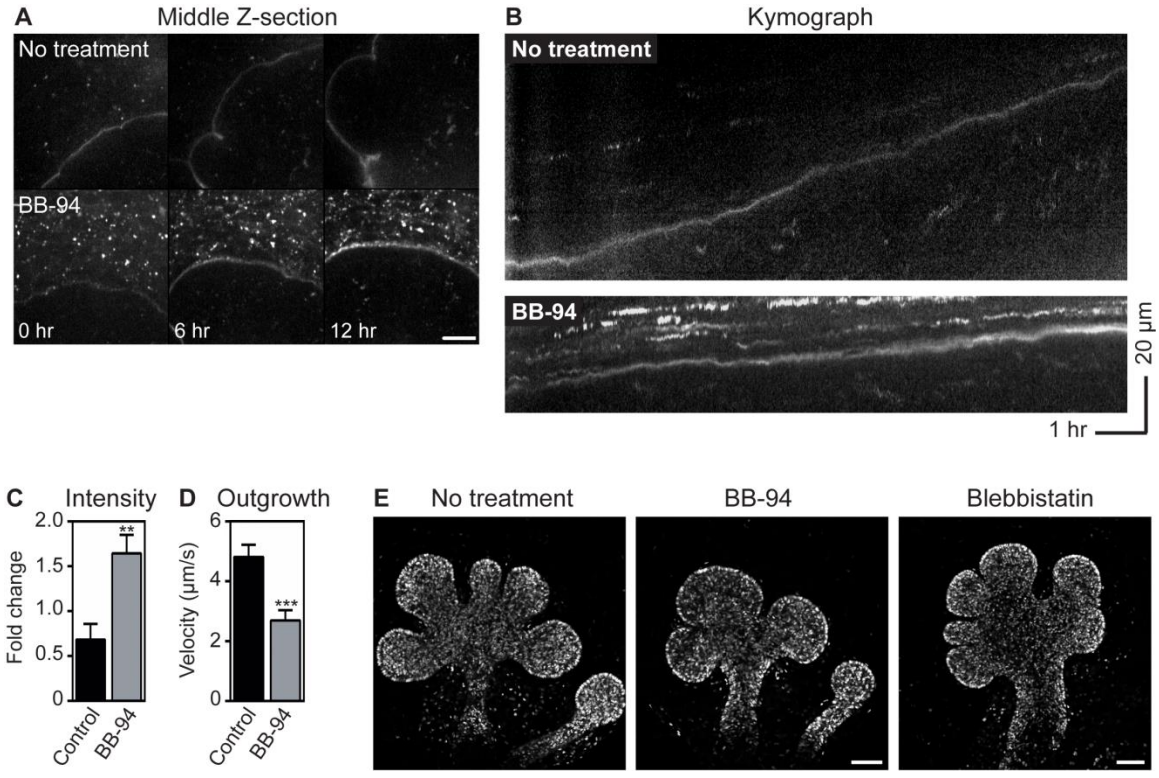


**Figure 3.7. Salivary gland bud outgrowth decreases as basement membrane accumulates**

Timelapse image through the middle of the bud (A) and 12 hour kymographs (B) of glands outgrown in E13 glands with or without 5 µM BB-94 and labeled with tagged collagen IV antibody to mark the basement membrane (BM); scale bar is 20 µm. (C) Fold change in basement membrane intensity (±SEM) after 12 hours of treatment with BB-94 compared with control in E13 SMGs. (D) Average bud outgrowth velocity (±SEM) after 12 hours of treatment with BB-94 (n= 4 experiments, 10 glands), **p<0.01, ***p<0.001, unpaired two-tailed t-test. (E) E12.5 salivary glands incubated overnight with or without 5 µM BB-94 or 50 µM blebbistatin and then exposed to EdU for 2 hours; scale bars are 100 µm.

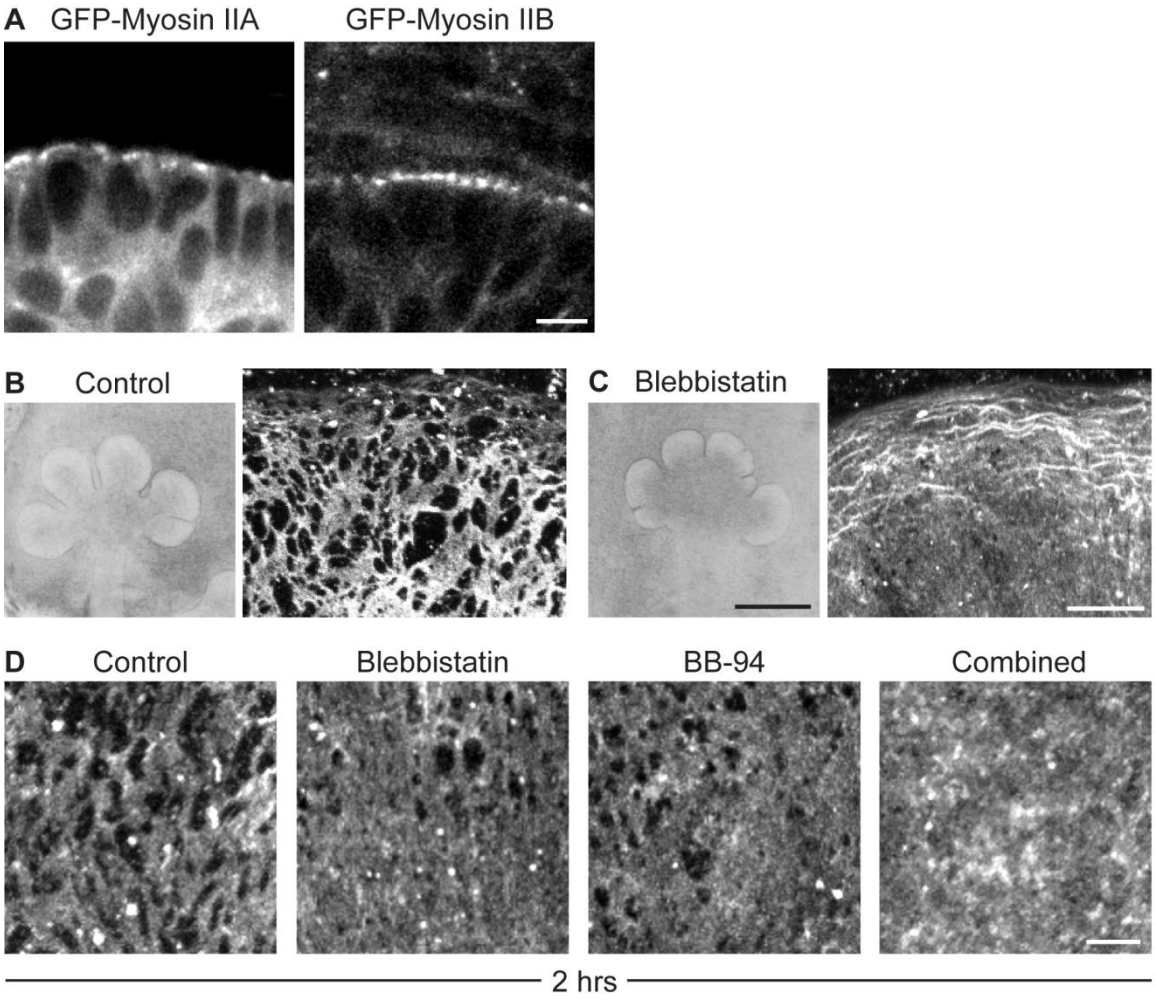


**Figure 3.8. Both protease and myosin II activity are required for the micro-perforations.**

(A) GFP-myosin IIA and IIB localization in an E13 salivary gland dissected from knock-in mice; scale bar is 10 μm. (B) Control and (C) 50 μM blebbistatin-treated E12.5 glands after 24 hours. Brightfield scale bar is 200 μm and collagen IV scale bar is 10 μm. (D) E13 salivary glands stained for collagen IV after 2 hour treatment with 50 μM blebbistatin, 5 μM BB-94, or both drugs together compared to control; scale bar is 5 μm.

# CHAPTER 4

## Rearward translocation of the basement membrane helps to shape branching of the developing salivary gland

### Preface

This chapter includes data from my first-authored paper entitled, "Local and global dynamics of the basement membrane during branching morphogenesis require protease activity and actomyosin contractility" that has been submitted and is under revision at the journal *Developmental Biology* and our un-published work on global basement membrane dynamics. We followed up on an observation of a phenomenon we noticed while performing live-imaging of the basement membrane for the micro-perforation project. The entire basement membrane seemed to move rearward slowly towards the duct, in addition to its rapid, local chaotic movements discussed in the previous chapter. Here, I explored this phenomenon under the supervision of my advisor, Kenneth Yamada.

## Introduction

The current assumption in the field is that rapid matrix synthesis and degradation are tightly regulated by an unknown mechanism to maintain a basement membrane around the expanding epithelium during branching morphogenesis. We showed in the previous chapter that part of this remodeling process included the formation of micro-perforations in the basement membrane, which allowed the tissue to expand within the confines of the matrix. In seminal work from the 1980s, Bernfield and Banerjee radio-labeled native glycosaminoglycans and performed pulse-chase experiments in the salivary gland that showed this basement membrane component incorporated first at the tips of the end buds and later accumulated in the cleft regions. The authors concluded that the rates of synthesis and degradation of the basement membrane differ in various regions of the epithelium; the deposition and degradation were high at the distal ends of the buds and low in the clefts (Bernfield and Banerjee, 1982). This observation still dominates the field today.

A more recent pulse-chase study using exogenous fibronectin with two fluorescent tags in cultures of isolated epithelia showed that older matrix ends up in the clefts. This finding suggests that the basement membrane does not merely undergo simple matrix proteolysis and deposition during branching, but that the matrix actually move into the clefts. This translocation of the matrix was originally proposed to accumulate fibronectin to guide cleft formation (Larsen et al., 2006). It was later shown that ROCK-mediated contractile forces were required to assemble fibronectin for cleft progression (Daley et al., 2009). We sought to describe the dynamics of the basement membrane translocation and hypothesized that the translocation is required not only to

guide cleft formation, but also to accumulate matrix to stabilize and sculpt the clefts and ducts.

## Results

With our fluorescently-labeled, non-perturbing collagen IV antibody and the iLAS FRAP system, we bleached a small line, approximately 7x60 pixels, parallel to the tip of the bud on the basement membrane of intact glands as a reference point to explore whether the matrix translocated during development. The glands were incubated with the antibody in media for at least 2 hours, and then the antibody was washed out of the dish and replaced with imaging media that was free of antibody. In the presence of antibody in the media, the bleach spot recovers quickly, making it impossible to track; without the antibody in the media, the bleached area remains visible for several hours. Kymographs were created of the bleached area, perpendicular to the tip of the bud, to measure the translocation velocity. We captured several Z-planes starting at the bottom surface of the salivary gland end bud and created maximum intensity projections, which enabled us to visualize a flat surface instead of a single line outlining the bud we would have seen if we had imaged the middle section of the bud. Imaging the lower portion of the bud also allowed us to image closer to the coverslip for crisper images and cleaner edges of the bleached regions.

### *The epithelium translocates the basement membrane towards the duct, where it accumulates*

We found that basement membrane translocates from at the tip of the E13 salivary gland toward the duct at a rate of 8.7 μm/hr (Fig. 4.1A and B). This translocation speed decreased when measured closer to the duct, consistent with the idea that the basement

membrane accumulates around the ducts, and its increase in thickness and loss of flexibility reduce the rate of translocation. The shape and size of a photobleached bleached region remains the same during translocation near the tip of the bud, but at the center of the bud, where the basement membrane has fewer micro-perforations, the bleached region appears to crumple and shrink (Fig. 4.1C). This observation suggests that the basement membrane compacts and builds up at the base of the buds. Immunostaining of perlecan, laminin, and collagen IV all showed increased staining at the center of the buds into the duct. In fact, the basement membrane appeared to accumulate into thick dense fibril-like structures beginning at the middle of the bud and extending into the ducts (Fig. 4.1D). We confirmed this observation with timelapse imaging. These fibrils were oriented perpendicular to the tip of the bud and parallel to the duct; similar accumulation was observed in the clefts. We also observed that the translocation speed decreased and the perforations disappeared at later stages of development. Preliminary data suggests similar basement membrane translocation and accumulation occur in the developing lung.

Next we hypothesized that the epithelial cells actively pull the basement membrane towards the duct, because the axial ratio (length/width) of the micro-perforations was on average 1.5 in all areas of the bud measured (Fig. 4.2B). This is the only measurement that did not change between the 4 regions of the end bud we analyzed. The perforations were elongated perpendicular to the tip of the bud, along the axis of translocation, as if they were being pulled and stretched lengthwise. We confirmed that the basement membrane could still translocate without the mesenchyme in epithelial rudiment culture, as previously reported (Fig. 4.2A) (Larsen et al., 2006). The

translocation was significantly slower compared to the intact gland, suggesting that mesenchymal growth factors may play a role in stimulating the rate of movement. However, the epithelium was still capable of pulling the basement membrane in a concerted manner towards the duct by itself without any mesenchyme.

Since the epithelium could translocate the basement membrane towards the duct on its own, the most obvious explanation was that the epithelial cells migrate together towards the duct, towing the basement membrane along with them in a mechanism similar to one described during mouse eyelid closure (Heller et al., 2014). We used the KikGR mice described in Chapter 2 to track the outer epithelial cells in conjunction with the labeled collagen IV antibody (Fig. 4.3A). We found that the individual epithelial cells migrate randomly along the basement membrane as we described in Chapter 2; they do not migrate collectively as an epithelial sheet (Fig. 4.3B). The cells were often associated with the basement membrane, but they do not migrate continuously or collectively towards the duct; in fact, we observe cells moving away from the duct as often as we observe cells moving toward it. Additionally, the migration speed of the epithelial cells associated with the basement membrane was much faster than the basement membrane translocation speed, 20 μm/hr (Fig. 2.3A) (Hsu et al., 2013) compared to 9 μm/hr, respectively. Thus, we conclude that the epithelial cells are not simply moving collectively towards the duct and towing the basement membrane along with them.

***Basement membrane translocation requires actomyosin contractility and cell-matrix adhesion***

Upon closer examination of mesenchyme-free cultures we observed that the basement membrane contracted just below the equator of the end buds. We observed

rapid increases in fluorescent intensity in small areas of the basement membrane, suggesting that the epithelial cells beneath the basement membrane were contracting it. Contraction of the basement membrane in this area may be responsible for generating the pulling force required for its translocation. We speculate that a highly contractile population of cells, at the base of the bud where the basement membrane begins to accumulate, provide the pulling force for the translocation of the basement membrane.

Because contractility could be involved in the translocation of the basement membrane, we treated the glands with the myosin II ATPase inhibitor, blebbistatin, and found that the translocation stopped almost immediately. The bleached area actually moved forward slightly, towards the tip with bud expansion at a rate of 2.5 μm/hr (Fig. 4.1B and 4.4B). There also was less accumulation of the basement membrane in the duct following blebbistatin treatment. In addition to actomyosin contractility, preliminary data show that cell attachment to the basement membrane is required for the translocation, since inhibitory antibodies to β1 integrin significantly slow the speed of translocation (Fig. 4.4A). Both treatments greatly reduced branching of the salivary gland, as previously shown in Chapter 2 (Hsu et al., 2013).

We also examined whether basement membrane flexibility had a role in the translocation of the basement membrane. Overnight treatment with the broad protease activity inhibitor BB-94 appeared to thicken and stiffen the basement membrane as we showed in Chapter 3; we found that the translocation was significantly slowed with this treatment to 1.7 μm/hr (Fig. 4.1B and 4.4C). BB-94 also inhibited branching of the gland, without decreasing cell proliferation. These findings suggest that local increased basement membrane flexibility has two purposes in the developing salivary gland, (1) to

allow controlled, directed expansion, as discussed in the previous chapter, and (2) to allow basement membrane translocation for structural stabilization.

**Discussion**

We have described novel cell-matrix dynamics in the developing salivary gland. In fact, we believe this dynamic movement can explain the findings reported by Bernfield and Bannerjee 1981. In their classic pulse-chase experiments, they found that the radioactivity was incorporated into the basement membrane at the tips of the buds first during the "pulse" and more slowly in the ducts and clefts during the "chase." This finding is exactly what we would expect if the basement membrane translocates into the duct regions. Our ability to perform florescent live organ imaging allowed us to visualize this process in 3D and in real time.

We have been unable to pinpoint the exact mechanism of the translocation, but we have been able to eliminate several potential mechanisms. Directed deposition of the basement membrane at the tip of the growing end bud could displace older matrix, pushing it towards the duct. We argue that the presence of the basement membrane micro-perforations and their elongated axial ratio eliminate this "pushing" hypothesis, because if matrix were to be pushed down over the bud, the micro-perforations would potentially fill in at the tip of the bud first, instead of at the middle of the bud. The long axis of the perforations would also be expected to be perpendicular to the orientation we observe. Moreover, blebbistatin, the myosin II ATPase inhibitor, halts the translocation. This finding suggests that the process is mechanically driven by actomyosin contraction instead of simple physical displacement of old matrix by newly deposited basement membrane (Fig. 4.4B). Additionally, with broad protease inhibition, the matrix appears to

accumulate evenly throughout the gland, not just at the tip of the bud; this observation indicates that matrix deposition occurs everywhere (Fig. 4.4C).

The basement membrane appears to be pulled and not pushed, since the micro-perforations were elongated along the axis perpendicular to the tip of the bud (Fig. 4.2B). We eliminated the possibility of highly motile outer bud cells at the tip of the bud providing the cells responsible for the directional movement of the matrix when we found that the cells did not migrate in concerted fashion towards the duct with the basement membrane in tow (Fig. 4.3).

If the cells are not towing the basement membrane towards the duct as they migrate, there may be a subset of cells that act in a coordinated fashion to translocate the basement membrane evenly, suggesting some form of planar cell polarity. We hypothesize that a highly contractile, polarized population of cells near the base of the bud translocates the basement membrane rearward. We have already been demonstrated that there are separate populations of cells within the epithelium of the salivary gland with different modes of migration (Hsu et al., 2013); Perhaps this subpopulation of cells has specific dynamics as well. We have observed cells contracting the matrix in epithelial rudiment culture, and these cells are likely not migratory since they are positioned at the beginning of the duct (Walker et al., 2008). Planar cell polarity is required during *Xenopus* convergent extension for cell polarization and indirectly in fibronectin fibril assembly; both pathways activate actomyosin contractility through Rho/ROCK or myosin regulatory light chain kinase, respectively (Davidson et al., 2008; Dzamba et al., 2009; Habas et al., 2001; Rozario et al., 2009; Skoglund and Keller, 2010). Perhaps a planar-polarized population of cells at the base of the bud is responsible for both polarization

and translocation of the basement membrane. Consequently, future investigation of non-canonical Wnt or other instigators of planar cell polarity in the translocation of the basement membrane seems warranted (Bilder and Haigo, 2012; Skoglund and Keller, 2010; Viktorinova et al., 2009).

Translocation of the basement membrane could explain why the micro-perforations disappear at the equator of the end buds. The largest circumference of the end bud is at the equator, and the surface area decreases beyond this point, closer to the duct. Thus, the sheet of basement membrane would crumple and accumulate/aggregate once it passes beyond the equator of the bud, because there would be excess material with less surface area to cover. Because the epithelial cells appear to be pulling the basement membrane rearward, we believe the matrix is under tension. We speculate that the force vectors change direction slightly once past the equator, as the decrease in surface area will pull them inward toward the duct instead of straight down prior to reaching the equator. These forces could help shape and stabilize the duct.

We also propose that the phenomenon of basement membrane translocation is important to accumulate matrix in the cleft and duct to stabilize these structures. Collagenase treatment has been shown previously to decrease branching by regression of established clefts and inhibition of new ones (Banerjee et al., 1977; Fukuda et al., 1988; Grobstein and Cohen, 1965). Furthermore, we speculate that the translocation could contribute to the remodeling of the basement membrane into the fibrils we observe. There have been a few instances in which epithelial cells exert physical forces to shape their surrounding extracellular matrix, inducing remodeling in *Drosophila* egg chamber elongation and mammary gland organoid culture (Haigo and Bilder, 2011; Tanner et al.,

2012; Wang et al., 2013). In the *Drosophila* egg chamber, the entire epithelium rotates to orient the stationary basement membrane into fibrils (Haigo and Bilder, 2011). This rotation requires polarized Misshapen to the rear of the cell, which decreases integrin levels to allow the rear of the cell to detach and facilitate cell migration (Lewellyn et al., 2013). Mammary gland acini rotate in basement membrane extract in an actomyosin-dependent manner (Wang et al., 2013). Conversely, in the salivary gland, the basement membrane moves and the cells are likely less coherently motile. Either way, coordinated attachment and detachment of the cells from the basement membrane, as in the *Drosophila* egg chamber, is required to enable the cells to translocate the matrix. The net result is similar, though the cells are probably stationary in the salivary gland, in generating an orientated matrix to shape and support morphogenesis.

In summary, we describe a novel basement membrane dynamic during salivary gland development. The epithelium translocates the basement membrane rearward, moving it towards the duct at an average rate of 9 μm/hr. We have preliminary evidence that the basement membrane translocates rearward in the embryonic lung as well, suggesting that this may be a broad mechanism used by branched organs. The basement translocation slows closer to the center of the bud, and the basement membrane accumulates to stabilize the ducts and clefts. The epithelium itself is capable of translocating the basement membrane, but the epithelial cells are not simply towing the matrix towards the duct as they migrate. Translocation is myosin II dependent and requires cell-matrix adhesion. Additionally, when the basement membrane is thicker and stiffer after treatment with a broad protease inhibitor, the translocation is slowed significantly. We hypothesize that the epithelial cells at the base of the bud are

mechanically pulling the basement membrane reward towards the duct. Further experiments are necessary to confirm the mechanism of this matrix translocation.

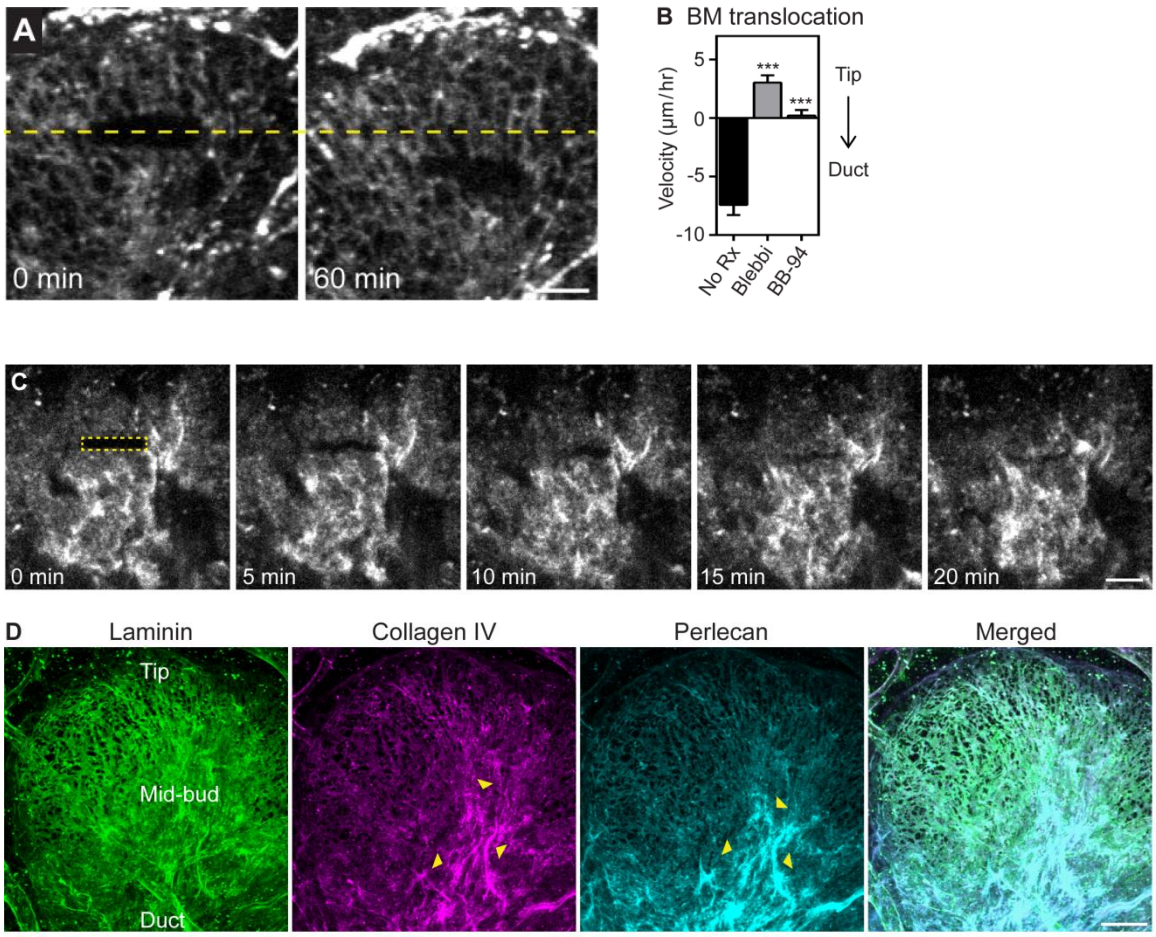


**Figure 4.1. The basement membrane translocates towards the duct where it accumulates.**

An E13 salivary gland was pre-incubated with fluorescently labeled collagen IV antibody and imaged without the labeled antibody in the media. A rectangular region was bleached near the tip of the end bud and imaged for 60 minutes; (A) shows the start and end images. The bleached region moved rearward, toward the duct; scale bar is 10 µm. The yellow dashed line indicates the starting point of the bleached region. (B) Directional quantification of translocation speed at the tip of the end buds with no treatment, 50 µM blebbistatin or 5 µM BB-94 treatment. (C) A bleached region near the equator of the bud, where there are fewer micro-perforations, crumples and nearly disappears after 20 minutes. Scale bar is 20 µm. (D) Immunostatining for laminin, collagen IV, and perlecan

show increased staining and an accumulation of basement membrane into fibril-like structures near the equator of the bud into the duct. Scale bar is 20 µm.

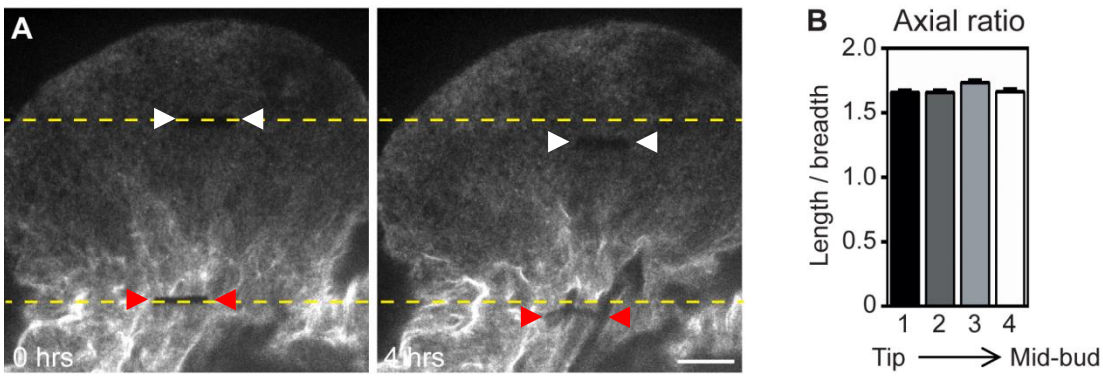


**Figure 4.2. The epithelium alone can pull the basement membrane rearward.**

(A) Epithelial rudiments from an E13 salivary gland translocate their endogenous basement membrane rearward; scale bar is 20 µm. Epithelia were pre-treated with labeled collagen IV antibody and then two regions were bleached, one near the tip of the bud (white arrowheads) and one in the duct (red arrowheads). The yellow dashed lines indicate the starting positions of the bleached regions. The bleached region in the duct crumples, while the one near the tip of the bud maintains its shape, as in the intact gland. (B) Axial ratios of the micro-perforations in the four zones characterized in the previous chapter, figure 3.4. The axial ratio did not differ between zones; they were all elongated perpendicular to the tip of the bud.

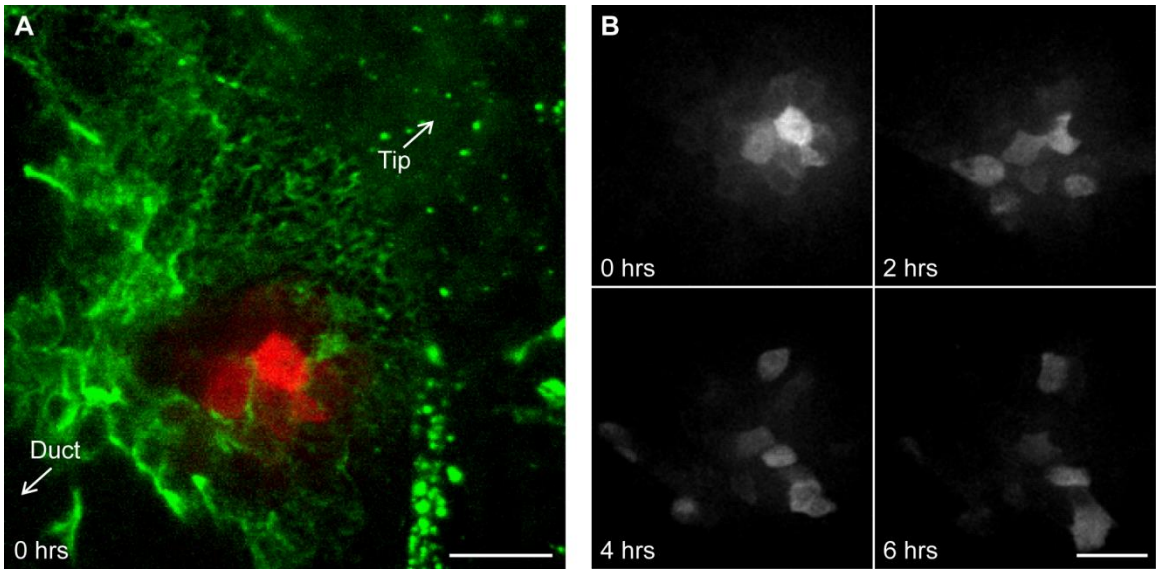


**Figure 4.3. The epithelial cells are not moving in concert towards the duct and simply towing the basement membrane rearward.**

(A) Using our KikGR transgenic mouse from Chapter 2, we photoconverted a subset of epithelial cells (red) in an E13 salivary gland and imaged at the bottom of the end bud to determine if the cells migrated towards the duct together. The basement membrane was imaged with a fluorescently labeled collagen IV antibody (green). (B) Time series of only the photoconverted epithelial cells over 6 hours. The cells move independently and do not all move towards the duct, located toward the lower left corner of the frame. Scale bars are 20 μm.

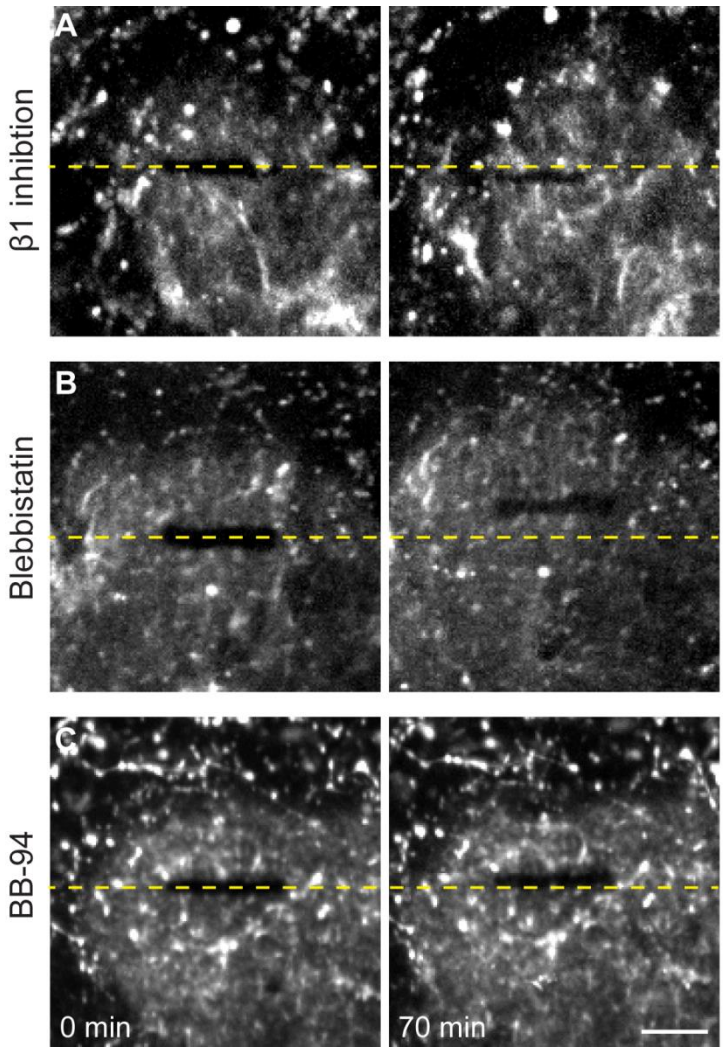


**Figure 4.4. Inhibition of cell-matrix adhesion, actomyosin contractility, and protease activity inhibit basement membrane translocation.**

E13 salivary glands were treated overnight with 100 µg/ml Ha 2/5 β1 inhibitory antibody (A), 50 µM blebbistatin (B), or 5 µM BB-94 (C), incubated with labeled collagen IV antibody and then imaged in antibody-free media. The bleached regions barely moved rearward toward the duct (oriented toward the bottom of the page) and in the case of blebbistatin treatment the bleached region moved forward slightly with bud outgrowth. Scale bar is 20 µm.

# CHAPTER 5

## Conclusions and perspective

Understanding the basic biology of developing organs is a key first step toward therapy of disease states and tissue engineering. Recapitulation of the developmental program or part of it de novo, is one of the potential ways in which we could eventually generate new organs to replace those that have been lost or damaged (Harunaga et al., 2011). The intrinsic dynamics of embryonic salivary gland epithelial cells (Hsu et al., 2013) and its surrounding basement membrane during normal morphogenesis suggests that salivary gland architecture is not fixed, but instead is highly plastic, involving significant motility of cells and basement membrane. Although obviously quite challenging, tissue engineering would take advantage of the sophisticated self-assembly mechanisms used in normal development to generate the vast numbers of acini of normal glands to provide enough epithelial surface area for adequate production of saliva.

In this dissertation, we sought to describe and understand the cell and basement membrane dynamics of branching morphogenesis using the mouse submandibular salivary gland as a model. While there are some differences in developmental mechanisms involving tissue patterning as well as hormonal and growth factor responses between branched organs (Andrew and Ewald, 2010; Fata et al., 2004), many aspects of previous research has been found to apply broadly across multiple organ systems, including cell motility during development as well as the importance of basement membrane proteins, actomyosin contractility, and protease activity (Kim and Nelson,

2012). We demonstrate that salivary gland development is remarkably dynamic, both in cell motility and cell-matrix interactions. Through the use of improved imaging techniques and equipment; we have been able to visualize, characterize, and experimentally analyze branching of intact organs in real time.

We have found that the epithelial cells in the developing salivary gland are highly motile, especially the outer bud cells in contact with the basement membrane relative to the inner bud cells, which suggests that the extracellular matrix may have a stimulatory effect on motility. Interestingly, the duct cells, which are also in contact with the basement membrane, do not migrate. How the basement membrane could have a stimulatory effect on the outer bud cells but not on the duct cells is unclear. The cells could be a distinct population that processes the extracellular signal differently, or the basement membrane itself could be different around the bud versus the duct and induce different cell behaviors.

It has been proposed that these extremely motile epithelial cells in the end buds of developing salivary and mammary glands undergo a partial epithelial-to-mesenchyme transition (EMT) (Chen et al., 2013; Lochter et al., 1997a; Lochter et al., 1997b; Onodera et al., 2010; Sternlicht et al., 1999). EMT in mammary epithelial cells was shown to be dependent on exposure to MMP3 and extracellular matrix proteins; in MMP3-stimulated cells, laminin was inhibitory while fibronectin promoted EMT (Chen et al., 2013; Park and Schwarzbauer, 2014). Interestingly, we and others have shown that MMP activity is high in the epithelial end buds of the salivary and mammary glands (Fata et al., 2004; Rebustini et al., 2009). Fibronectin is a basement membrane-associated protein, not typically found in the basement membrane; consistent with this concept, our laboratory

finds by immunostaining that fibronectin does not co-localize with the typical basement membrane components, instead it often localizes slightly above the basement membrane on the mesenchymal side. The presence of the micro-perforations in the basement membrane only at the tip of the end buds could allow the outer bud cells more contact with fibronectin, stimulating their motility. Addition of exogenous fibronectin to intact embryonic salivary glands has been shown to increase branching morphogenesis (Onodera et al., 2010; Sakai et al., 2003), perhaps by locally increasing epithelial cell motility through a partial EMT. The ductal cells could be less exposed to proteases and fibronectin, since there are significantly fewer holes in the basement membrane surrounding the duct, and basement membrane components including laminin accumulate into fibril-like structures around the duct. Thus the cells in the duct could be less motile due to a lack of protease activity and fibronectin exposure as well as increased exposure to laminin to inhibit EMT.

We also find that the basement membrane itself is highly dynamic; it is constantly remodeled by local proteolysis or physical movement and accumulation throughout development to shape and support the architecture of the gland. This gives rise to local differences in basement membrane structure, composition, and distensibility that can differentially mediate cell behavior. Because the epithelial cells are so motile, the remodeling of the basement membrane must be carefully controlled to maintain a barrier between the epithelial compartment and the surrounding stroma. We have found that the basement membrane is perforated by hundreds of tiny holes at the tip of the epithelial buds. These microscopic holes allow for physical contact between the epithelium and mesenchyme while maintaining a barrier between the two compartments. The large

numbers of perforations and their location also increase basement membrane distensibility specifically at the tip of the buds to permit controlled, local epithelial expansion. Additionally, the basement membrane perforations probably allow for increased growth factor release and diffusion, driving motility and proliferation specifically at the tip of the epithelial buds.

In addition to the local perforations of the basement membrane, we found that the entire basement membrane translocates rearward towards the duct. Interestingly, both protease and myosin II activity are required for formation and maintenance of the basement membrane perforations as well as basement membrane translocation, suggesting a link between the two processes. We believe that this link is the distensibility of the basement membrane; the perforations increase the distensiblity of the basement membrane to allow the epithelium to expand rapidly, and at the same time, the epithelial cells to pull the basement membrane rearwards to accumulate locally in order to stabilize the duct (Fig. 5.1). The local and global basement membrane dynamics halt immediately after myosin II inhibition or after overnight treatment with broad protease inhibition. This difference in inhibition time suggests that proteases increase matrix distensibility, allowing cells to physically pull and remodel it through actomyosin contractility. We speculate that general protease activity weakens the basement membrane at the tip of the bud and the underlying epithelial cells punch through the basement membrane, and then myosin II-mediated pulling of the basement membrane stretches and elongates the perforations as the basement membrane is translocated. Translocation of the basement membrane allows it to accumulate around the ducts in fibril-like structures, changing the

composition, topography, and distensibility of the basement membrane. This change could stabilize the tissue by signaling to decrease cell motility as discussed above.

Here we have described a dynamic, bidirectional system in which the cells modify the basement membrane, which in turn affects cell behavior and matrix remodeling to sculpt tissue architecture in the branching of the embryonic mouse salivary gland. Interestingly, degradation of the basement membrane and EMT are key steps in cancer metastasis (Radisky and Radisky, 2010). Perhaps this normal developmental system is up-regulated in disease states, allowing for activation and escape of epithelial cells through the basement membrane. There are still several questions to address. In bidirectional systems such as this one, there is always the classic chicken-and-egg question of what comes first? Do the cells change their behavior first to remodel the basement membrane or does the organization of the matrix, perhaps mediated by the mesenchyme where the majority of fibronectin is secreted, trigger changes in cell behavior? More specifically, we wonder which proteases are responsible for basement membrane perforations and how their activity is restricted just to the tips of the end buds? Unfortunately this question is particularly difficult to answer, since our data indicate that multiple proteases are involved, there are so many proteases with redundant activities, and targeted gene knock-down is especially tricky in our three dimensional, mammalian organ system; further examination would likely require a reductionist approach in organoid or cell cultures systems. The mechanism of translocation of the basement membrane is also unknown.

We hope to conduct two-photon laser ablation experiments that may indicate that the basement membrane is under tension, indicating that it is being pulled. Additionally,

we could potentially laser ablate the contractile cells near the base of the bud to determine if they are responsible for the movement of the matrix. Nevertheless, our studies have already successfully established that (1) there are distinct populations of cells within the epithelium of the salivary gland that have different modes of migration, (2) the basement membrane is perforated at the tips of the end buds, locally increasing its distensibility to potentially allow expansion of the epithelium, (3) the basement membrane is highly dynamic, exhibiting local and global remodeling, and (4) the basement membrane is pulled rearward by the epithelium to stabilize the duct.

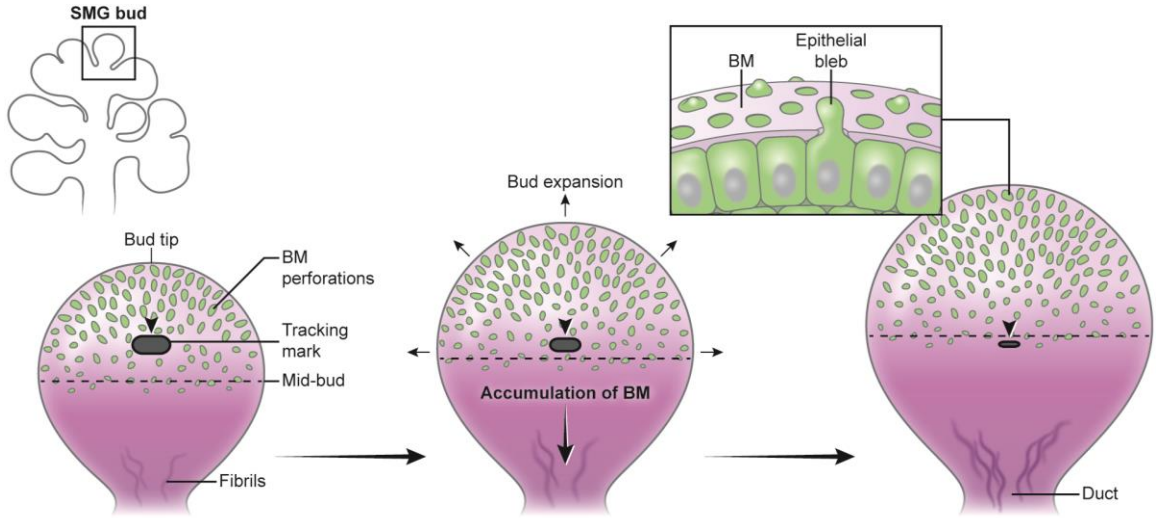


**Figure 5.1. A model of basement membrane dynamics.**

The basement membrane, displayed in magenta, surrounding the tips of expanding salivary gland epithelial end buds becomes perforated with numerous holes that decrease in size and number closer to the middle of the bud. These micro-perforations are likely formed by a combination of proteases degrading the basement membrane, epithelial cell protrusions extending through the basement membrane (shown in green) and making contact with the mesenchyme (not pictured), as well as both local and global myosin II mediated contraction of the basement membrane. The presence of the micro-perforations increases the distensibility of the basement membrane, allowing for outgrowth of the epithelium and myosin II mediated rearward translocation and accumulation of the basement membrane. Protease activity and actomyosin contractility are required for the local and global remodeling of the basement membrane during development of the salivary gland.

## MATERIALS AND METHODS

### Dissection and ex vivo organ culture

Salivary submandibular glands (or simply termed salivary glands) were dissected from the following mouse strains at embryonic day 12.5 (E12.5; E0 is defined as the day of conception and observation of a vaginal plug): wild-type ICR (Harlan), homozygous eGFP-myosin IIA knock-in transgenic (B6, 129, BALB) (Zhang et al., 2012), homozygous eGFP-myosin IIB knock-in transgenic (C57BL6 and 129Sv, MMRRC, ID# 37053) (Fischer et al., 2009) or homozygous KikGR expressing transgenic (FVB and B6;129S4). The myosin II knock-in mice were generated in the laboratory of Robert Adelstein (NHLBI) and bred in-house. The KikGR transgenic mice were generated by our laboratory and the NIDCR gene targeting core. All mice were housed, bred, and euthanized according to an approved NIDCR animal study protocol. The dissected glands were placed on 0.1 μm pore polycarbonate membrane filters (Sterlitech) floating on 200 μl media in a 50 mm dish with 14 mm glass bottom (MatTek Corp.). Complete media contained DMEM/F12 phenol-red free medium plus L-glutamine and HEPES (Gibco) containing 100 U/ml penicillin, 100 μg/ml streptomycin, 150 μg/ml vitamin C, and 50 μg/ml transferrin. Glands were cultured for 18-24 hours in 5% $CO_2$ at 37°C. For the developmental time point analysis, the salivary glands were dissected at the specified embryonic day and cultured for 2 hours before immunostaining. Embryonic lung and kidney were dissected at E11 and cultured in the same way. For live imaging, the glands were cultured on 0.2 μm pore filters (Whatman).

**Inhibitors**

For drug treatments, glands were cultured in the media described above with 50 μM blebbistatin, 5 μM batimastat (BB-94), 25 μM GM6001 [Ilomastat] MMP inhibitor, or 20 μM Y-27632 all from Millipore/Calbiochem. These drugs were re-suspended in DMSO or water, and treated glands were exposed to ≤ 0.025% DMSO, which we had previously determined to have no effect on salivary gland morphology and development. For inhibitory antibody treatments, glands were cultured in complete media with the addition of 100 mg/ml of ECCD-1 (Invitrogen) for E-cadherin inhibition or 100 mg/ml Ha2/5 (BD Biosciences) for β1 integrin inhibition or 100 mg/ml each of Ha2/5 and GoH3 (BD Biosciences) for β1 and α6 integrin inhibition. Recombinant TIMP-2 (Calbiochem) and TIMP-3 (R&D systems) were re-suspended in PBS, and glands were cultured with each inhibitory protein at a final concentration of 4 μg/ml in complete media.

**Epithelial rudiment dissection**

Salivary glands were dissected as described above and submerged in 3 mg/ml dispase I (Gibco) at 37°C for 20 minutes to dissolve the basement membrane. The glands were rinsed twice with 10% BSA and placed in a pyrex spot plate with BSA. The mesenchyme was mechanically dissected away from the epithelium with forceps. The epithelia were rinsed with media and placed in 3 mg/ml laminin gel (Cultrex) on top of a 0.1 μm or 0.2 μm pore polycarbonate membrane filter for either fixed immunofluorescence or live imaging respectively. The filter floated on top of complete media, as described above, supplemented with 200 ng/ml EGF and 50μg/ml FGF7. The epithelial rudiments were incubated for 48 hours in 5% $CO_2$ at 37°C prior to imaging to allow the basement membrane to reassemble.

**Immunostaining**

Immunostaining was performed as previously described (Onodera et al., 2010). Primary antibodies were used at the following concentrations: anti-collagen IV (Millipore) 2 µg/ml, anti-laminin (Sigma) 3 µg/ml, anti-perlecan (Millipore) 5 µg/ml, or anti-E-cadherin ECCD-2 (Invitrogen) 5 µg/ml. Secondary antibodies were species-specific donkey anti-IgG Cy2, Cy3, and Cy5-labeled antibodies from Jackson ImmunoResearch used at a concentration of 4 µg/ml. Imaging was performed using a Zeiss 710 laser scanning confocal microscope with a 40X (1.3 NA) Plan-Apochromat oil objective as previously described (Hsu et al., 2013). All images displayed in the figures are representative of at least 4 separate experiments, with 2-4 glands each.

**Perforation area analysis**

Confocal Z-stacks were acquired at 0.38 µm intervals starting at the mid-point of the end bud to the bottom of the bud from submandibular salivary glands fixed and stained for collagen IV and analyzed using the 710 confocal microscope. Maximum projections of these Z-stacks were created, and four symmetric, rectangular regions from the tip of the bud to the center of the bud were marked. These regions occupied approximately 2/3 of an axis running perpendicular to the tip of the bud, bisecting the center of the bud and ending at the bottom of the bud where the secondary duct began. Each region was thresholded for dark objects in MetaMorph and manually adjusted for optimal inclusion of the majority of the perforations. Masked objects that were touching the edge of the region were not included in the measurements, except for the percent perforated measurements – all objects were included in this count. Perforation area was determined by MetaMorph software's region measurements function. Any perforations

missed by this automated procedure (due to appearing lighter than others) were manually traced, but they comprised less than 10% of the total perforation area.

**Antibody conjugation**

Collagen IV antibodies (Millipore) were first concentrated to >1.5mg/ml prior to the addition of a 7-fold molar excess of Alexa Fluor 647 NHS-ester dye (Invitrogen) solubilized in DMSO (Sigma-Aldrich). The antibody-dye mixture was gently rotated at 4°C for 2 hours. Excess dye was removed with buffer exchange columns (Pierce) against PBS (HyClone) (Hsu et al., 2013).

**KikGR photoconversion and live imaging**

E13 salivary glands from KikGR mice were dissected and cultured overnight, then inverted such that the glands faced the 14 mm coverslip of a 35 mm MatTek dish and secured with vacuum grease (Dow Corning). Standard media as described above plus OxyFluor (Oxyrase) and 2.5 μg/ml labelled collagen IV antibody was then added. The glands were allowed to incubate for approximately 5-8 hours before imaging up to 20 hours after the addition of inhibitors. For blebbistatin treatment, cells were first photoconverted, then this inhibitor was added immediately prior to imaging; for all other experiments, treatment was initiated immediately after affixing the glands to the glass-bottom dish.

For photo-conversion, an iLAS FRAP module (Roper Scientific Europe) was used together with a 50 mW 405 nm diode laser (CrystaLaser) on our spinning disc confocal microscope. The “FRAP on the fly” module was used with an 8 pixel diameter with an output power of 20%. Cells were photo-converted until 561 nm images demonstrated a

large dynamic range at 14-bits, with the average light exposure being between 10-20 seconds. This photo-conversion method using a focused beam of laser illumination resulted in multiple cells being photo-converted in a column, with the Z-section height dependent on the numerical aperture of the objective.

Images for each emission channel were acquired over a total Z-section of 20 µm (Z-spacing of 2 µm) every 10 minutes for up to 12 hours. Salivary glands were imaged with 488 nm, 561 nm and 642 nm excitation wavelengths, except for experiments with blebbistatin where only 561 nm and 642 nm excitation lines with used. Prior to photoconversion, the glands were bleached with 100% 561 nm laser light for 20 seconds to reduce background noise. Exposure times for each channel were set to between 300-600 milliseconds depending on brightness. Laser power settings were set to 12%, 18%, and 8%, for 488 nm, 561 nm, and 642 nm excitation lines, respectively.

**Basement membrane and GFP live imaging**

The majority of the live-organ imaging was performed using a CSU-Z1 spinning disc confocal (Yokogawa) on a Axiovert 200M microscope (Zeiss) with either a EM-CCD camera (Photometrics) or a sCMOS camera (Hamamatsu) using a 40X C-Apochromat water objective (NA 1.2) or a 63X Plan-Apochromat oil objective (NA 1.4). The laser rig, lasers, stage, chamber, and software were exactly the same as described previously (Hsu et al., 2013). Laser power settings were set to 15% for 488 nm and 10-20% for 647 nm. Exposure times were between 200-800 milliseconds for each channel. Gland imaging times ranged from 20 minutes to 12 hours, and intervals varied between 5 seconds to 10 minutes depending on the experiment. We did not image longer than 12 hours, because under these conditions, gland morphology begins to change after 24 hours

submerged in media. Additionally a LSM 510 NLO META confocal microscope (Zeiss) was also used with the same 40X water objective listed above for live imaging of the organs from the GFP knock-in mice. We imaged with non-descanned detectors and a 1.5 W two-photon laser (Coherent) tuned to 850 nm at 9% power.

**Basement membrane photobleaching**

Salivary glands or epithelial rudiments were dissected and cultured and placed on 0.2 μm as described above. The filter and glands were inverted so that the salivary glands faced the cover glass of a MatTek dish; the filter was secured to the glass with vacuum grease along the periphery of the filter. Glands were cultured in standard media plus OxyFluor (Oxyrase) and 5 μg/ml 647- labeled collagen IV antibody for at least 2 hours. The glands were rinsed and submerged in complete media without antibody for imaging. The iLAS FRAP module was also used for photo-bleaching of the fluorescent collagen IV antibody. A 7x60 pixel box was drawn parallel to the tip of the bud and bleached at 55% power for 3 seconds. Using a 40X C-Apochromat water objective (NA 1.2) we imaged intact glands for 1 hour at 5 minute intervals and epithelial rudiments for at least 4 hours at 10-minute intervals since the basement membrane translocates significantly slower in this condition.

For inhibitory treatments, the glands were treated overnight with BB-94 and it was present in all subsequent media; for integrin inhibition, the gland were incubated with the inhibitory β1 antibody when the glands were flipped and tacked down for imaging with the labeled collagen IV antibody and the inhibitory antibody was present in the media throughout imaging. For the blebbistatin treatment, the glands were treated after bleaching and prior to imaging.

**Bud expansion analysis**

ICR mouse salivary glands were cultured on 0.2 μm filters overnight and mounted for imaging as described above; glands were cultured in standard media plus OxyFluor (Oxyrase) and 5 μg/ml 647- labeled collagen IV antibody for 2-5 hours. We then added either 1 ml of medium alone or 1 ml of medium containing 10 μM BB-94 for control or drug treatment experiments respectively, which diluted the final antibody concentration to 2.5 μg/ml and BB-94 to 5 μM. The glands were imaged for 12 hours at 1-minute intervals at either 0.5 or 1 μm Z intervals for up to 30 planes (from the bottom of the bud to the middle of the bud), for a total of 721 time points on the spinning disc microscope. The last plane of the stack (mid-point of the bud) images was analyzed. In MetaMorph, each stack was segmented into ten 72-image stacks for kymograph analysis. A kymograph was generated for each segment for which a single non-segmented line could be drawn perpendicular to the basement membrane and parallel to bud outgrowth. One line was drawn per bud, and the lines were drawn through the apex of the bud. From the kymographs, the slope and the velocity were determined by drawing a single non-segmented line from the top of the kymograph to the bottom along the basement membrane.

**Basement membrane intensity analysis**

From the same movies analyzed for bud expansion, we were able to quantify change in basement membrane intensity. A circular region with an area of 26 $\mu m^2$ was drawn at the basement membrane along the kymograph lines at the first time point and the last time point at 12 hours. A background area was also sampled immediately behind the basement membrane area within the bud for each time point. The average intensities

of each area were determined by MetaMorph's region statistics function at the starting and ending time points. The background intensity was subtracted from the basement membrane intensity and normalized such that the starting point was one and the ending point represents fold change in intensity.

**Basement membrane distensibility analysis**

E12 ICR submandibular salivary glands were cultured overnight on 0.2 μm filters as described above. The glands were then inverted and submerged face-down in complete media containing 5 μg/ml labeled collagen IV antibody for 5 hours; the filters were attached using vacuum grease. A subset of glands was pre-treated with 50 μM blebbistatin in addition to the labeled antibody. Other glands were pre-treated overnight with 5 μM BB-94 and then incubated with labeled antibody. The glands were then rinsed with media to remove any unbound antibody, and the glands were detached from the filter and placed on a glass slide with a 13 mm diameter, 0.12 mm depth imaging spacer (Grace Bio-labs) in a drop of fresh complete medium with or without the desired drug treatment; a 1-thickness coverslip was then used to seal this slide chamber. In this enclosed imaging configuration, where the glands were as flat as possible without any polycarbonate filter to scatter light, we were able to image for a maximum of 3 hours with the 63X C-Apochromat water objective (NA 1.2). The glands were imaged for every 10 seconds for 20 minutes total at 0.5 μm Z intervals, with a maximum of 55 Z-planes needed to image one-half of the bud.

The stack was compressed into a maximum projection image in MetaMorph, and 136 $\mu m^2$ regions were chosen for analysis from the tip or from the middle of the bud in untreated controls, or only from the tip areas in the glands that had been treated with

either blebbistatin or BB-94. These regions were chosen based on these locations and the abundance of fiduciary marks to track. The natural accumulations of labeled antibody on the surface of the basement membrane were tracked individually using the track points application in MetaMorph in 'blinded' fashion. Between 2 and 6 points were tracked per region. The XY coordinates were exported and the distance between points in every possible combination per region was calculated. The minimum distance was subtracted from the maximum distance between points to determine the distensibility of the basement membrane at that region during the 20-minute assay period.

**EdU proliferation analysis**

Salivary glands were dissected at E12.5 and cultured overnight in the presence of the specified drug treatment. The following morning, one half the media is replaced containing 2 μM Click-iT EdU (Invitrogen) and the drug treatment for two hours. The glands are fixed, permeablized, blocked and stained for total nuclei with DAPI (Invitrogen) according to the provided Invitrogen protocol. The glands are imaged on a Zeiss 710 laser scanning confocal with a 10X (0.45 NA) Plan Apochromat air or 40X (1.3 NA) Plan_Apochromat oil objective. Quantification was performed on the three middle sections aquired with the 40X objective, 5 μm apart to minimize overlap of nuclei. The MetaMorph function, equalize light, was applied to normalize all the grey values in the stack. A region was drawn around the epithelium in the middle slice of the DAPI section and copied into the EdU sections such that the same area was measured for each channel, and then the images were manually thresholded to highlight the nuclei. The thresholded area was calculated with the region measurements function and the

thresholded area for each EdU section is divided by the corresponding thresholded area of total nuclei to get a ratio of EdU positive nuclei.

**Translocation velocity analysis**

Maximum projection images are created in MetaMorph and then a line was drawn perpendicularly through the bleached bar, starting at the tip of the bud and moving back towards the duct, and a kymograph was created. From the kymograph, the slope and the velocity were determined by drawing a single non-segmented line from the top of the kymograph to the bottom along the edge of the bleached bar.

# REFERENCES


Adelstein, R.S., and M.A. Conti. 1975. Phosphorylation of platelet myosin increases actin-activated myosin ATPase activity. *Nature*. 256:597-8.

Andrew, D.J., and A.J. Ewald. 2010. Morphogenesis of epithelial tubes: Insights into tube formation, elongation, and elaboration. *Dev Biol*. 341:34-55.

Artym, V.V., Y. Zhang, F. Seillier-Moiseiwitsch, K.M. Yamada, and S.C. Mueller. 2006. Dynamic interactions of cortactin and membrane type 1 matrix metalloproteinase at invadopodia: defining the stages of invadopodia formation and function. *Cancer Res*. 66:3034-43.

Banerjee, S.D., R.H. Cohn, and M.R. Bernfield. 1977. Basal lamina of embryonic salivary epithelia. Production by the epithelium and role in maintaining lobular morphology. *J Cell Biol*. 73:445-63.

Bernfield, M., and S.D. Banerjee. 1982. The turnover of basal lamina glycosaminoglycan correlates with epithelial morphogenesis. *Dev Biol*. 90:291-305.

Bilder, D., and S.L. Haigo. 2012. Expanding the morphogenetic repertoire: perspectives from the Drosophila egg. *Dev Cell*. 22:12-23.

Bluemink, J.G., P. Van Maurik, and K.A. Lawson. 1976. Intimate cell contacts at the epithelial/mesenchymal interface in embryonic mouse lung. *J Ultrastruct Res*. 55:257-70.

Candiello, J., G.J. Cole, and W. Halfter. 2010. Age-dependent changes in the structure, composition and biophysical properties of a human basement membrane. *Matrix Biol*. 29:402-10.

Chen, Q.K., K. Lee, D.C. Radisky, and C.M. Nelson. 2013. Extracellular matrix proteins regulate epithelial-mesenchymal transition in mammary epithelial cells. *Differentiation*. 86:126-32.

Colognato, H., D.A. Winkelmann, and P.D. Yurchenco. 1999. Laminin polymerization induces a receptor-cytoskeleton network. *J Cell Biol*. 145:619-31.

Cutler, L.S. 1977. Intercellular contacts at the epithelial-mesenchymal interface of the developing rat submandibular gland in vitro. *J Embryol Exp Morphol*. 39:71-7.

Cutler, L.S. 1980. The dependent and independent relationships between cytodifferentiation and morphogenesis in developing salivary gland secretory cells. *Anat Rec*. 196:341-7.

Cutler, L.S. 1990. The role of extracellular matrix in the morphogenesis and differentiation of salivary glands. *Adv Dent Res*. 4:27-33.

Cutler, L.S., and A.P. Chaudhry. 1973. Intercellular contacts at the epithelial-mesenchymal interface during the prenatal development of the rat submandibular gland. *Dev Biol*. 33:229-40.

Daley, W.P., E.M. Gervais, S.W. Centanni, K.M. Gulfo, D.A. Nelson, and M. Larsen. 2012. ROCK1-directed basement membrane positioning coordinates epithelial tissue polarity. *Development*. 139:411-22.

Daley, W.P., K.M. Gulfo, S.J. Sequeira, and M. Larsen. 2009. Identification of a mechanochemical checkpoint and negative feedback loop regulating branching morphogenesis. *Dev Biol*. 336:169-82.

Daley, W.P., J.M. Kohn, and M. Larsen. 2011. A focal adhesion protein-based mechanochemical checkpoint regulates cleft progression during branching morphogenesis. *Dev Dyn*. 240:2069-83.

Daley, W.P., S.B. Peters, and M. Larsen. 2008. Extracellular matrix dynamics in development and regenerative medicine. *J Cell Sci*. 121:255-64.

Daley, W.P., and K.M. Yamada. 2013. ECM-modulated cellular dynamics as a driving force for tissue morphogenesis. *Curr Opin Genet Dev*. 23:408-14.

Davidson, L.A., B.D. Dzamba, R. Keller, and D.W. Desimone. 2008. Live imaging of cell protrusive activity, and extracellular matrix assembly and remodeling during morphogenesis in the frog, Xenopus laevis. *Dev Dyn*. 237:2684-92.

Doyle, A.D., F.W. Wang, K. Matsumoto, and K.M. Yamada. 2009. One-dimensional topography underlies three-dimensional fibrillar cell migration. *J Cell Biol*. 184:481-90.

Dzamba, B.J., K.R. Jakab, M. Marsden, M.A. Schwartz, and D.W. DeSimone. 2009. Cadherin adhesion, tissue tension, and noncanonical Wnt signaling regulate fibronectin matrix organization. *Dev Cell*. 16:421-32.

Even-Ram, S., A.D. Doyle, M.A. Conti, K. Matsumoto, R.S. Adelstein, and K.M. Yamada. 2007. Myosin IIA regulates cell motility and actomyosin-microtubule crosstalk. *Nat Cell Biol*. 9:299-309.

Ewald, A.J., A. Brenot, M. Duong, B.S. Chan, and Z. Werb. 2008. Collective epithelial migration and cell rearrangements drive mammary branching morphogenesis. *Dev Cell*. 14:570-81.

Ewald, A.J., R.J. Huebner, H. Palsdottir, J.K. Lee, M.J. Perez, D.M. Jorgens, A.N. Tauscher, K.J. Cheung, Z. Werb, and M. Auer. 2012. Mammary collective cell migration involves transient loss of epithelial features and individual cell migration within the epithelium. *J Cell Sci*. 125:2638-54.

Fata, J.E., Z. Werb, and M.J. Bissell. 2004. Regulation of mammary gland branching morphogenesis by the extracellular matrix and its remodeling enzymes. *Breast Cancer Res*. 6:1-11.

Fischer, R.S., M. Gardel, X. Ma, R.S. Adelstein, and C.M. Waterman. 2009. Local cortical tension by myosin II guides 3D endothelial cell branching. *Curr Biol*. 19:260-5.

Fukuda, Y., Y. Masuda, J. Kishi, Y. Hashimoto, T. Hayakawa, H. Nogawa, and Y. Nakanishi. 1988. The role of interstitial collagens in cleft formation of mouse embryonic submandibular gland during initial branching. *Development*. 103:259-67.

Gill, S.E., M.C. Pape, and K.J. Leco. 2006. Tissue inhibitor of metalloproteinases 3 regulates extracellular matrix--cell signaling during bronchiole branching morphogenesis. *Dev Biol*. 298:540-54.

Gjorevski, N., and C.M. Nelson. 2009. Bidirectional extracellular matrix signaling during tissue morphogenesis. *Cytokine Growth Factor Rev*. 20:459-65.

Grobstein, C. 1953. Morphogenetic interaction between embryonic mouse tissues separated by a membrane filter. *Nature*. 172:869-70.

Grobstein, C., and J. Cohen. 1965. Collagenase: effect on the morphogenesis of embryonic salivary epithelium in vitro. *Science*. 150:626-8.

Gutzeit, H.O., W. Eberhardt, and E. Gratwohl. 1991. Laminin and basement membrane-associated microfilaments in wild-type and mutant Drosophila ovarian follicles. *J Cell Sci*. 100:781-8.

Habas, R., Y. Kato, and X. He. 2001. Wnt/Frizzled activation of Rho regulates vertebrate gastrulation and requires a novel Formin homology protein Daam1. *Cell*. 107:843-54.

Hagedorn, E.J., H. Yashiro, J.W. Ziel, S. Ihara, Z. Wang, and D.R. Sherwood. 2009. Integrin acts upstream of netrin signaling to regulate formation of the anchor cell's invasive membrane in C. elegans. *Dev Cell*. 17:187-98.

Hagedorn, E.J., J.W. Ziel, M.A. Morrissey, L.M. Linden, Z. Wang, Q. Chi, S.A. Johnson, and D.R. Sherwood. 2013. The netrin receptor DCC focuses invadopodia-driven basement membrane transmigration in vivo. *J Cell Biol*. 201:903-13.

Haigo, S.L., and D. Bilder. 2011. Global tissue revolutions in a morphogenetic movement controlling elongation. *Science*. 331:1071-4.

Halfter, W., J. Candiello, H. Hu, P. Zhang, E. Schreiber, and M. Balasubramani. 2013. Protein composition and biomechanical properties of in vivo-derived basement membranes. *Cell Adh Migr*. 7:64-71.

Harunaga, J., J.C. Hsu, and K.M. Yamada. 2011. Dynamics of salivary gland morphogenesis. *J Dent Res*. 90:1070-7.

Heller, E., K.V. Kumar, S.W. Grill, and E. Fuchs. 2014. Forces generated by cell intercalation tow epidermal sheets in Mammalian tissue morphogenesis. *Dev Cell*. 28:617-32.

Hieda, Y., K. Iwai, T. Morita, and Y. Nakanishi. 1996. Mouse embryonic submandibular gland epithelium loses its tissue integrity during early branching morphogenesis. *Dev Dyn*. 207:395-403.

Hinck, L., and G.B. Silberstein. 2005. Key stages in mammary gland development: the mammary end bud as a motile organ. *Breast Cancer Res*. 7:245-51.

Hiramatsu, R., T. Matsuoka, C. Kimura-Yoshida, S.W. Han, K. Mochida, T. Adachi, S. Takayama, and I. Matsuo. 2013. External mechanical cues trigger the establishment of the anterior-posterior axis in early mouse embryos. *Dev Cell*. 27:131-44.

Holmbeck, K., P. Bianco, J. Caterina, S. Yamada, M. Kromer, S.A. Kuznetsov, M. Mankani, P.G. Robey, A.R. Poole, I. Pidoux, J.M. Ward, and H. Birkedal-Hansen. 1999. MT1-MMP-deficient mice develop dwarfism, osteopenia, arthritis, and connective tissue disease due to inadequate collagen turnover. *Cell*. 99:81-92.

Horne-Badovinac, S. 2014. The Drosophila Egg Chamber-A New Spin on How Tissues Elongate. *Integr Comp Biol. DOI: 10.1093/icb/icu067*.

Hsu, J.C., H. Koo, J.S. Harunaga, K. Matsumoto, A.D. Doyle, and K.M. Yamada. 2013. Region-specific epithelial cell dynamics during branching morphogenesis. *Dev Dyn*. 242:1066-77.

Hynes, R.O., and A. Naba. 2012. Overview of the matrisome--an inventory of extracellular matrix constituents and functions. *Cold Spring Harb Perspect Biol*. 4:a004903.

Ihara, S., E.J. Hagedorn, M.A. Morrissey, Q. Chi, F. Motegi, J.M. Kramer, and D.R. Sherwood. 2011. Basement membrane sliding and targeted adhesion remodels tissue boundaries during uterine-vulval attachment in Caenorhabditis elegans. *Nat Cell Biol*. 13:641-51.

Joo, E.E., and K.M. Yamada. 2014. MYPT1 regulates contractility and microtubule acetylation to modulate integrin adhesions and matrix assembly. *Nat Commun*. 5:3510.

Kadoya, Y., K. Kadoya, M. Durbeej, K. Holmvall, L. Sorokin, and P. Ekblom. 1995. Antibodies against domain E3 of laminin-1 and integrin alpha 6 subunit perturb branching epithelial morphogenesis of submandibular gland, but by different modes. *J Cell Biol*. 129:521-34.

Kadoya, Y., M. Nomizu, L.M. Sorokin, S. Yamashina, and Y. Yamada. 1998. Laminin alpha1 chain G domain peptide, RKRLQVQLSIRT, inhibits epithelial branching morphogenesis of cultured embryonic mouse submandibular gland. *Dev Dyn*. 212:394-402.

Kadoya, Y., and S. Yamashina. 1993. Distribution of alpha 6 integrin subunit in developing mouse submandibular gland. *J Histochem Cytochem*. 41:1707-14.

Kadoya, Y., and S. Yamashina. 2010. Cellular dynamics of epithelial clefting during branching morphogenesis of the mouse submandibular gland. *Dev Dyn*. 239:1739-47.

Kallman, F., and C. Grobstein. 1965. Source of Collagen at Epitheliomesenchymal Interfaces during Inductive Interaction. *Dev Biol*. 11:169-83.

Kashimata, M., and E.W. Gresik. 1997. Epidermal growth factor system is a physiological regulator of development of the mouse fetal submandibular gland and regulates expression of the alpha6-integrin subunit. *Dev Dyn*. 208:149-61.

Kelley, L.C., L.L. Lohmer, E.J. Hagedorn, and D.R. Sherwood. 2014. Traversing the basement membrane in vivo: a diversity of strategies. *J Cell Biol*. 204:291-302.

Kerosuo, L., and M. Bronner-Fraser. 2012. What is bad in cancer is good in the embryo: importance of EMT in neural crest development. *Semin Cell Dev Biol*. 23:320-32.

Khoshnoodi, J., V. Pedchenko, and B.G. Hudson. 2008. Mammalian collagen IV. *Microsc Res Tech*. 71:357-70.

Kim, H.Y., and C.M. Nelson. 2012. Extracellular matrix and cytoskeletal dynamics during branching morphogenesis. *Organogenesis*. 8:56-64.

Komuro, T. 1985. Fenestrations of the basal lamina of intestinal villi of the rat. Scanning and transmission electron microscopy. *Cell Tissue Res*. 239:183-8.

Landsverk, M.L., and H.F. Epstein. 2005. Genetic analysis of myosin II assembly and organization in model organisms. *Cell Mol Life Sci*. 62:2270-82.

Larsen, M., C. Wei, and K.M. Yamada. 2006. Cell and fibronectin dynamics during branching morphogenesis. *J Cell Sci*. 119:3376-84.

Lehtonen, E. 1975. Epithelio-mesenchymal interface during mouse kidney tubule induction in vivo. *J Embryol Exp Morphol*. 34:695-705.

Lelongt, B., G. Trugnan, G. Murphy, and P.M. Ronco. 1997. Matrix metalloproteinases MMP2 and MMP9 are produced in early stages of kidney morphogenesis but only MMP9 is required for renal organogenesis in vitro. *J Cell Biol*. 136:1363-73.

Lerner, D.W., D. McCoy, A.J. Isabella, A.P. Mahowald, G.F. Gerlach, T.A. Chaudhry, and S. Horne-Badovinac. 2013. A Rab10-dependent mechanism for polarized basement membrane secretion during organ morphogenesis. *Dev Cell*. 24:159-68.

Lewellyn, L., M. Cetera, and S. Horne-Badovinac. 2013. Misshapen decreases integrin levels to promote epithelial motility and planar polarity in Drosophila. *J Cell Biol*. 200:721-9.

Li, S., P. Liquari, K.K. McKee, D. Harrison, R. Patel, S. Lee, and P.D. Yurchenco. 2005. Laminin-sulfatide binding initiates basement membrane assembly and enables receptor signaling in Schwann cells and fibroblasts. *J Cell Biol*. 169:179-89.

Limouze, J., A.F. Straight, T. Mitchison, and J.R. Sellers. 2004. Specificity of blebbistatin, an inhibitor of myosin II. *J Muscle Res Cell Motil*. 25:337-41.

Lochter, A., S. Galosy, J. Muschler, N. Freedman, Z. Werb, and M.J. Bissell. 1997a. Matrix metalloproteinase stromelysin-1 triggers a cascade of molecular alterations that leads to stable epithelial-to-mesenchymal conversion and a premalignant phenotype in mammary epithelial cells. *J Cell Biol*. 139:1861-72.

Lochter, A., A. Srebrow, C.J. Sympson, N. Terracio, Z. Werb, and M.J. Bissell. 1997b. Misregulation of stromelysin-1 expression in mouse mammary tumor cells accompanies acquisition of stromelysin-1-dependent invasive properties. *J Biol Chem*. 272:5007-15.

Lu, P., K. Takai, V.M. Weaver, and Z. Werb. 2011. Extracellular matrix degradation and remodeling in development and disease. *Cold Spring Harb Perspect Biol*. 3.

Mammoto, T., and D.E. Ingber. 2010. Mechanical control of tissue and organ development. *Development*. 137:1407-20.

McKee, K.K., D. Harrison, S. Capizzi, and P.D. Yurchenco. 2007. Role of laminin terminal globular domains in basement membrane assembly. *J Biol Chem*. 282:21437-47.

Melnick, M., and T. Jaskoll. 2000. Mouse submandibular gland morphogenesis: a paradigm for embryonic signal processing. *Crit Rev Oral Biol Med*. 11:199-215.

Menko, A.S., J.A. Kreidberg, T.T. Ryan, E. Van Bockstaele, and M.A. Kukuruzinska. 2001. Loss of alpha3beta1 integrin function results in an altered differentiation program in the mouse submandibular gland. *Dev Dyn*. 220:337-49.

Metzger, R.J., O.D. Klein, G.R. Martin, and M.A. Krasnow. 2008. The branching programme of mouse lung development. *Nature*. 453:745-50.

Metzger, R.J., and M.A. Krasnow. 1999. Genetic control of branching morphogenesis. *Science*. 284:1635-9.

Mollard, R., and M. Dziadek. 1998. A correlation between epithelial proliferation rates, basement membrane component localization patterns, and morphogenetic potential in the embryonic mouse lung. *Am J Respir Cell Mol Biol*. 19:71-82.

Moore, K.A., T. Polte, S. Huang, B. Shi, E. Alsberg, M.E. Sunday, and D.E. Ingber. 2005. Control of basement membrane remodeling and epithelial branching morphogenesis in embryonic lung by Rho and cytoskeletal tension. *Dev Dyn*. 232:268-81.

Nakanishi, Y., H. Nogawa, Y. Hashimoto, J. Kishi, and T. Hayakawa. 1988. Accumulation of collagen III at the cleft points of developing mouse submandibular epithelium. *Development*. 104:51-9.

Nakanishi, Y., F. Sugiura, J. Kishi, and T. Hayakawa. 1986. Collagenase inhibitor stimulates cleft formation during early morphogenesis of mouse salivary gland. *Dev Biol*. 113:201-6.

Nakaya, Y., and G. Sheng. 2009. An amicable separation: Chick's way of doing EMT. *Cell Adh Migr*. 3:160-3.

Oblander, S.A., Z. Zhou, B.G. Galvez, B. Starcher, J.M. Shannon, M. Durbeej, A.G. Arroyo, K. Tryggvason, and S.S. Apte. 2005. Distinctive functions of membrane type 1 matrix-metalloprotease (MT1-MMP or MMP-14) in lung and submandibular gland development are independent of its role in pro-MMP-2 activation. *Dev Biol*. 277:255-69.

Onodera, T., T. Sakai, J.C. Hsu, K. Matsumoto, J.A. Chiorini, and K.M. Yamada. 2010. Btbd7 regulates epithelial cell dynamics and branching morphogenesis. *Science*. 329:562-5.

Ortega, N., and Z. Werb. 2002. New functional roles for non-collagenous domains of basement membrane collagens. *J Cell Sci*. 115:4201-14.

Park, J., and J.E. Schwarzbauer. 2014. Mammary epithelial cell interactions with fibronectin stimulate epithelial-mesenchymal transition. *Oncogene*. 33:1649-57.

Patel, V.N., S.M. Knox, K.M. Likar, C.A. Lathrop, R. Hossain, S. Eftekhari, J.M. Whitelock, M. Elkin, I. Vlodavsky, and M.P. Hoffman. 2007. Heparanase cleavage of perlecan heparan sulfate modulates FGF10 activity during ex vivo submandibular gland branching morphogenesis. *Development*. 134:4177-86.

Patel, V.N., K.M. Likar, S. Zisman-Rozen, S.N. Cowherd, K.S. Lassiter, I. Sher, E.A. Yates, J.E. Turnbull, D. Ron, and M.P. Hoffman. 2008. Specific heparan sulfate structures modulate FGF10-mediated submandibular gland epithelial morphogenesis and differentiation. *J Biol Chem*. 283:9308-17.

Patel, V.N., I.T. Rebustini, and M.P. Hoffman. 2006. Salivary gland branching morphogenesis. *Differentiation*. 74:349-64.

Petrie, R.J., N. Gavara, R.S. Chadwick, and K.M. Yamada. 2012. Nonpolarized signaling reveals two distinct modes of 3D cell migration. *J Cell Biol*. 197:439-55.

Pflicke, H., and M. Sixt. 2009. Preformed portals facilitate dendritic cell entry into afferent lymphatic vessels. *J Exp Med*. 206:2925-35.

Plosa, E.J., K.A. Gooding, R. Zent, and L.S. Prince. 2012. Nonmuscle myosin II regulation of lung epithelial morphology. *Dev Dyn*. 241:1770-81.

Poschl, E., U. Schlotzer-Schrehardt, B. Brachvogel, K. Saito, Y. Ninomiya, and U. Mayer. 2004. Collagen IV is essential for basement membrane stability but dispensable for initiation of its assembly during early development. *Development*. 131:1619-28.

Radisky, E.S., and D.C. Radisky. 2010. Matrix metalloproteinase-induced epithelial-mesenchymal transition in breast cancer. *J Mammary Gland Biol Neoplasia*. 15:201-12.

Rebustini, I.T., C. Myers, K.S. Lassiter, A. Surmak, L. Szabova, K. Holmbeck, V. Pedchenko, B.G. Hudson, and M.P. Hoffman. 2009. MT2-MMP-dependent release of collagen IV NC1 domains regulates submandibular gland branching morphogenesis. *Dev Cell*. 17:482-93.

Rebustini, I.T., V.N. Patel, J.S. Stewart, A. Layvey, E. Georges-Labouesse, J.H. Miner, and M.P. Hoffman. 2007. Laminin alpha5 is necessary for submandibular gland epithelial morphogenesis and influences FGFR expression through beta1 integrin signaling. *Dev Biol*. 308:15-29.

Rizzo, M.A., M.W. Davidson, and D.W. Piston. 2009. Fluorescent protein tracking and detection: fluorescent protein structure and color variants. *Cold Spring Harb Protoc*. 2009:pdb top63.

Rowe, R.G., and S.J. Weiss. 2008. Breaching the basement membrane: who, when and how? *Trends Cell Biol*. 18:560-74.

Rowe, R.G., and S.J. Weiss. 2009. Navigating ECM barriers at the invasive front: the cancer cell-stroma interface. *Annu Rev Cell Dev Biol*. 25:567-95.

Rozario, T., and D.W. DeSimone. 2010. The extracellular matrix in development and morphogenesis: a dynamic view. *Dev Biol*. 341:126-40.

Rozario, T., B. Dzamba, G.F. Weber, L.A. Davidson, and D.W. DeSimone. 2009. The physical state of fibronectin matrix differentially regulates morphogenetic movements in vivo. *Dev Biol*. 327:386-98.

Saitoh, M., T. Ishikawa, S. Matsushima, M. Naka, and H. Hidaka. 1987. Selective inhibition of catalytic activity of smooth muscle myosin light chain kinase. *J Biol Chem*. 262:7796-801.

Sakai, T., M. Larsen, and K.M. Yamada. 2003. Fibronectin requirement in branching morphogenesis. *Nature*. 423:876-81.

Schuger, L., S. O'Shea, J. Rheinheimer, and J. Varani. 1990. Laminin in lung development: effects of anti-laminin antibody in murine lung morphogenesis. *Dev Biol*. 137:26-32.

Schwartz, M.A. 2010. Integrins and extracellular matrix in mechanotransduction. *Cold Spring Harb Perspect Biol*. 2:a005066.

Shakya, R., T. Watanabe, and F. Costantini. 2005. The role of GDNF/Ret signaling in ureteric bud cell fate and branching morphogenesis. *Dev Cell*. 8:65-74.

Sherwood, D.R., and P.W. Sternberg. 2003. Anchor cell invasion into the vulval epithelium in C. elegans. *Dev Cell*. 5:21-31.

Silberstein, G.B., and C.W. Daniel. 1982. Glycosaminoglycans in the basal lamina and extracellular matrix of the developing mouse mammary duct. *Dev Biol*. 90:215-22.

Simoes Sde, M., A. Mainieri, and J.A. Zallen. 2014. Rho GTPase and Shroom direct planar polarized actomyosin contractility during convergent extension. *J Cell Biol*. 204:575-89.

Skoglund, P., and R. Keller. 2010. Integration of planar cell polarity and ECM signaling in elongation of the vertebrate body plan. *Curr Opin Cell Biol*. 22:589-96.

Slavkin, H.C., and P. Bringas, Jr. 1976. Epithelial-mesenchyme interactions during odontogenesis. IV. Morphological evidence for direct heterotypic cell-cell contacts. *Dev Biol*. 50:428-42.

Spooner, B.S., and J.M. Faubion. 1980. Collagen involvement in branching morphogenesis of embryonic lung and salivary gland. *Dev Biol*. 77:84-102.

Sternlicht, M.D., H. Kouros-Mehr, P. Lu, and Z. Werb. 2006. Hormonal and local control of mammary branching morphogenesis. *Differentiation*. 74:365-81.

Sternlicht, M.D., A. Lochter, C.J. Sympson, B. Huey, J.P. Rougier, J.W. Gray, D. Pinkel, M.J. Bissell, and Z. Werb. 1999. The stromal proteinase MMP3/stromelysin-1 promotes mammary carcinogenesis. *Cell*. 98:137-46.

Tanner, K., H. Mori, R. Mroue, A. Bruni-Cardoso, and M.J. Bissell. 2012. Coherent angular motion in the establishment of multicellular architecture of glandular tissues. *Proc Natl Acad Sci U S A*. 109:1973-8.

Thompson, H.A., and B.S. Spooner. 1982. Inhibition of branching morphogenesis and alteration of glycosaminoglycan biosynthesis in salivary glands treated with beta-D-xyloside. *Dev Biol*. 89:417-24.

Timpl, R., and M. Dziadek. 1986. Structure, development, and molecular pathology of basement membranes. *Int Rev Exp Pathol*. 29:1-112.

Trier, J.S., C.H. Allan, D.R. Abrahamson, and S.J. Hagen. 1990. Epithelial basement membrane of mouse jejunum. Evidence for laminin turnover along the entire crypt-villus axis. *J Clin Invest*. 86:87-95.

Tsutsui, H., S. Karasawa, H. Shimizu, N. Nukina, and A. Miyawaki. 2005. Semi-rational engineering of a coral fluorescent protein into an efficient highlighter. *EMBO Rep*. 6:233-8.

Uehata, M., T. Ishizaki, H. Satoh, T. Ono, T. Kawahara, T. Morishita, H. Tamakawa, K. Yamagami, J. Inui, M. Maekawa, and S. Narumiya. 1997. Calcium sensitization of smooth muscle mediated by a Rho-associated protein kinase in hypertension. *Nature*. 389:990-4.

Vicente-Manzanares, M., X. Ma, R.S. Adelstein, and A.R. Horwitz. 2009. Non-muscle myosin II takes centre stage in cell adhesion and migration. *Nat Rev Mol Cell Biol*. 10:778-90.

Viktorinova, I., T. Konig, K. Schlichting, and C. Dahmann. 2009. The cadherin Fat2 is required for planar cell polarity in the Drosophila ovary. *Development*. 136:4123-32.

Walker, J.L., A.S. Menko, S. Khalil, I. Rebustini, M.P. Hoffman, J.A. Kreidberg, and M.A. Kukuruzinska. 2008. Diverse roles of E-cadherin in the morphogenesis of the submandibular gland: insights into the formation of acinar and ductal structures. *Dev Dyn*. 237:3128-41.

Wang, H., S. Lacoche, L. Huang, B. Xue, and S.K. Muthuswamy. 2013. Rotational motion during three-dimensional morphogenesis of mammary epithelial acini relates to laminin matrix assembly. *Proc Natl Acad Sci U S A*. 110:163-8.

Wei, C., M. Larsen, M.P. Hoffman, and K.M. Yamada. 2007. Self-organization and branching morphogenesis of primary salivary epithelial cells. *Tissue Eng*. 13:721-35.

Wessells, N.K., and J.H. Cohen. 1968. Effects of collagenase on developing epithelia in vitro: lung, ureteric bud, and pancreas. *Dev Biol*. 18:294-309.

Wiseman, B.S., M.D. Sternlicht, L.R. Lund, C.M. Alexander, J. Mott, M.J. Bissell, P. Soloway, S. Itohara, and Z. Werb. 2003. Site-specific inductive and inhibitory activities of MMP-2 and MMP-3 orchestrate mammary gland branching morphogenesis. *J Cell Biol*. 162:1123-33.

Yan, L., M.A. Moses, S. Huang, and D.E. Ingber. 2000. Adhesion-dependent control of matrix metalloproteinase-2 activation in human capillary endothelial cells. *J Cell Sci*. 113 ( Pt 22):3979-87.

Yurchenco, P.D. 2011. Basement membranes: cell scaffoldings and signaling platforms. *Cold Spring Harb Perspect Biol*. 3: a004911.

Zhang, Y., M.A. Conti, D. Malide, F. Dong, A. Wang, Y.A. Shmist, C. Liu, P. Zerfas, M.P. Daniels, C.C. Chan, E. Kozin, B. Kachar, M.J. Kelley, J.B. Kopp, and R.S. Adelstein. 2012. Mouse models of MYH9-related disease: mutations in nonmuscle myosin II-A. *Blood*. 119:238-50.